U.S.NRC

United States Nuclear Regulatory Commission

Protecting People and the Environment

PREDICTING HIGH ENERGY ARCING FAULT ZONES OF INFLUENCE FOR ALUMINUM USING AN ARC FLASH MODELING APPROACH

Evaluation of a model bias, uncertainty, parameter sensitivity and zone of influence estimation

Final

Prepared by:
G. Taylor[1]
C. LaFleur[2]

[1] U.S. Nuclear Regulatory Commission
[2] Sandia National Laboratories

Mark Henry Salley, NRC Project Manager

Research Information Letter
Office of Nuclear Regulatory Research

Disclaimer

ABSTRACT

This report documents the development of an arc flash hazard model to calculate the incident energy and zone of influence from high energy arcing faults (HEAFs) involving aluminum. The NRC has identified the potential for HEAFs involving aluminum to increase the damage zone beyond what is currently postulated in fire probabilistic risk assessment (PRA) methodologies. To estimate the hazard from HEAFs involving aluminum an arc flash model was developed. Differences between the initial model and nuclear power plant (NPP) fire PRA scenarios were identified. Modification of the initial model established from existing literature and test data was used to minimize these differences. The developed model was evaluated against NRC datasets to understand the model prediction and relative uncertainties. Finally, a range of fire PRA zone of influences (ZOI) were developed based on the developed model, target fragility estimates and update HEAF PRA methodology. The results were developed to support an NRC LIC-504 evaluation in tandem with other modeling efforts. The report documents the effort and provides a reference for any future advancements in arc flash modeling.

TABLE OF CONTENTS

LIST OF TABLES

LIST OF FIGURES

EXECUTIVE SUMMARY

PRIMARY AUDIENCE: Fire protection, electrical and probabilistic risk assessment engineers conducting or reviewing fire risk assessments related to high energy arcing faults.

SECONDARY AUDIENCE: Engineers, reviewers, utility managers, and other stakeholders who conduct, review, or manage fire protection programs and need to understand the underlying technical basis for the hazards associated with high energy arcing faults.

KEY RESEARCH QUESTION: How do you calculate the zone of influence for a high energy arcing fault (HEAF) involving aluminum?

RESEARCH OVERVIEW

Operating experience has shown that HEAFs pose a hazard to the safe operation of nuclear facilities. Current regulations and probabilistic risk assessment methods were developed using limited information, and uncertainties require the use of safety margins to bound the hazard. Testing aimed at providing additional data to improve realism identified a concern that HEAFs involving aluminum may increase the hazard potential. Testing identified that the presence of aluminum during a HEAF may increase the hazard potential.

Upon discovery of the potential hazard posed by aluminum, the NRC staff entered the issue into the NRC's generic issues (GI) process and informed licensees of relevant operating experienced in Information Notice 2017-004 [1]. The NRC GI process identified a need for specific data of HEAF tests involving aluminum which were performed in 2018 on medium-voltage switchgear and in 2019 on low-voltage switchgear and simplified box tests at medium-and low-voltage levels. Planned testing on medium-voltage bus ducts and other equipment was postponed due to the COVID-19 pandemic. To make progress with available test data and complete the risk assessment of the concern, an analytical effort was performed to develop revised zone of influences (ZOI) based on available data and literature.

This report documents the results of developing an arc flash hazard calculation to predict incident energy at various distances. The initial model is modified due to identified differences between model and fire PRA assumptions. This resulted in a modified model that is evaluated against NRC data to understand model bias and relative uncertainty. Using the modified model and target fragility estimates, ZOI estimates were developed.

KEY FINDINGS

This research yields an simple empirically-based approach to estimate the zone of influence for equipment containing aluminum components. Development and use of this approach identified the following key findings:

- The initial model underpredicts the aluminum test data for open box test configurations

- The initial model underpredicts the incident energy for longer duration switchgear tests (where the exothermic aluminum reaction was observed). The initial model overpredicts short duration tests, which is contributed to the lack of observed aluminum oxidation reaction and differences in model assumptions and tests data.

- Gap analysis identified a need to modify the model to account for enclosure breach characteristics. The time to breach an electrical enclosure from a HEAF source can be estimated based on existing models from gas insulated substation research, with modification based on geometrical differences.

    o The time to breach is dependent on enclosure material. Aluminum enclosures will breach approximately 4 times faster than a steel enclosure of equivalent thickness and fault current.

    o Additional time is required for the initial breach opening to enlarge for sufficient energy transfer to the targets. This can be estimated by analyzing existing data sets.

- Generator decay profiles for specific scenarios can be approximated by a constant current (shorter duration) profile that conserves energy.

- A sensitivity study found that the modified model is

    o relatively insensitive to the conductor spacing, enclosure volume and system voltage

    o moderately sensitive to the arcing current

    o has a linear relationship with the arc duration

    o model configuration has an impact on the model output

- Zone of influences (ZOIs) were developed based on the modified model and target fragility estimates with the following results. These ZOI estimates do not include any contribution from an ensuing fire.

    o Non-segregated bus duct

        ▪ The spherical ZOI increases from the current guidance (0.46 m [1.5 ft]) for most scenarios. The largest ZOI involves aluminum bus duct with a targeted aluminum bus duct which is estimated at 1.2 m (4 ft).

    o Medium-voltage switchgear

        ▪ Increase in ZOI estimates over current guidance was predicted for some scenarios. The lower target fragility category (15 MJ/m^2) had an upper predicted ZOI of 1.6 m (5.4 ft), while the higher target fragility category (30 MJ/m^2) had a marginal increase for only a few of the longest fault current scenarios 1.1 m (3.6 ft).

    o Low-voltage switchgear

        ▪ No scenarios involved the ZOI exceeding the current fire PRA guidance of 0.91 m (3 ft).

WHY THIS MATTERS

This report provides a numerical approach to estimate the zone of influence for HEAFs involving aluminum. This report represents an informational input to support NRC activities to understand how HEAFs are evaluated in NPP risk assessment to ensure the public's health and safety.

HOW TO APPLY RESULTS

Engineers performing fire probabilistic risk assessment method advancements involving aluminum HEAFs should focus on Section 4 of this report.

LEARNING AND ENGAGEMENT OPPORTUNITIES

Users of this report may be interested in the following learning opportunities:

Nuclear Energy Agency (NEA) HEAF Project to conduct experiments in order to explore the basic configurations, failure modes and effects of HEAF events. Primary objectives include (1) development of a peer-reviewed guidance document that could be readily used to assist regulators of participants, and (2) joint nuclear safety project report covering all testing and data captured. More information on the project and opportunities to participate in the program can be found online at https://www.oecd-nea.org/.

ACKNOWLEDGMENTS

1 INTRODUCTION

Events such as fires at a nuclear power plant can pose a significant risk to safe plant operations when consequences of fires are not mitigated. Licensees combat this risk by having robust fire protection programs designed to minimize the likelihood and consequences of fire. These programs provide reasonable assurance of adequate protection from known fire hazards. However, several hazards remain subject to a large degree of uncertainty, requiring significant safety margins in plant analyses.

One such infrequent hazard comprises an electrical arcing fault involving electrical distribution equipment and components comprised of aluminum. While the electrical faults and subsequent fires are considered in existing fire protection programs, recent research [1] has indicated that the presence of aluminum during the electrical fault can exacerbate the damage potential of the event. The extended damage capacity could exceed the protection provided by existing fire protection features for specific fire scenarios and increase plant risk estimated in fire probabilistic risk assessments (PRAs).

The U.S. Nuclear Regulatory Commission (NRC) Office of Nuclear Regulatory Research (RES) studies fire and explosion hazards to the safe operation of nuclear facilities. This includes developing data, tools and methodologies to support risk and safety assessments.

1.1   Background

HEAFs are hazardous events in which an electrical arc leads to the rapid release of energy in the form of heat, vaporized metal, and mechanical force. The guidance for modeling HEAF events in fire probabilistic risk assessments (PRA) is documented in Appendix M of NUREG/CR-6850, "EPRI/NRC-RES Fire PRA Methodology for Nuclear Power Facilities [2]." This guidance postulates that HEAFs can occur in switchgear, load centers, and bus ducts with a nominal voltage of 440V and above, and defines a zone of influence (ZOI) in which targets are assumed to be damaged.

An OECD/NEA report [3], published in June of 2013, documented 48 HEAF events, accounting for approximately 10% of the total fire events reports in the international fire records exchange program database. These events were often accompanied by loss of essential power and complicated shutdowns. To confirm the PRA methodology in NUREG/CR-6850, which was formulated based on limited observational data, the NRC led an international experimental campaign from 2014 to 2016 [4]. The results of these experiments uncovered an unexpected hazard posed by aluminum components in or near electrical equipment and the potential for unanalyzed equipment failures, which the current PRA modeling guidance does not address.

Upon discovery of the potential hazard posed by aluminum, the NRC's Office of Nuclear Reactor Regulation conducted an immediate safety evaluation and concluded that no immediate safety concern exists, but recommended that the NRC's Office of Nuclear Regulatory Research (RES) begin the generic issues (GI) process. Additionally, RES staff conducted a review of operating experience, and identified six events from the U.S. operating fleet where aluminum-related effects like those observed in testing were present. To inform licensees about the findings of this review and results of testing, the NRC issued Information Notice 2017-004 [1].

NRC-RES staff proposed this potential safety concern as a GI in a letter dated May of 2016 [5]. The Generic Issue Review Panel (GIRP) completed its screening evaluation [6] for proposed Generic Issue (GI) PRE-GI-018, "High-Energy Arc Faults (HEAFs) Involving Aluminum," and concluded that the proposed issue met all seven screening criteria outlined in Management Directive (MD) 6.4, "Generic Issues Program." Therefore, the GIRP recommended that this issue continue into the Assessment Stage of the GI program. The assessment plan, published in August of 2018 [7] and revised in 2019 [8], requires the NRC to develop updated PRA tools and methods for HEAFs to be used in pilot plant studies and risk evaluation. In August of 2021, the NRC determined that the issue no longer met the timeliness criterion of the generic issue program [9]. The NRC decided to continue to evaluate the issue by applying the NRC LIC-504, "Integrated Risk-Informed Decision-making Process for Emergent Issues" [10].

1.2 Overview of HEAF Research

The objective of the NRC's HEAF research program is to develop tools and methods to assess the risk posed by high energy arcing fault events based on experimental data, operating experience, and engineering judgment. These tools and methods will account for the primary factors that influence the occurrence and severity of HEAF events, including the presence of aluminum and plant electrical configuration and protection schemes.

To leverage the expertise of collaborative partners, NRC-RES and the Electric Power Research Institute (EPRI) formed a joint working group under the NRC-RES/EPRI memorandum of understanding (MOU). This working group has developed a list of tasks needed to support advancements to modeling HEAF in fire PRAs. One of these tasks includes development and validation of a HEAF hazard model. The working group has collaboratively focused on using computational fluid dynamic tools to estimate the HEAF hazard. This report provides an alternative approach using a modified empirically derived approach. The work documented in this report was prepared by NRC staff, with PRA scenario development support from Sandia National Laboratories.

1.3 Objective

The objective of this report is to document how an arc flash model [11], is developed for the application needs of the NRCs assessment of high energy arcing faults (HEAFs) involving aluminum. This report also documents model bias and uncertainty, along with a parameter sensitivity evaluation of the modified model.

1.4 Scope

The scope of this hazard modeling sub-task is to

1. present an overview of the initial arc flash model,
2. identify differences between the model and HEAF probabilistic risk assessment (PRA) scenarios
3. provide basis for modification to model
4. evaluate the final model against empirical data available to the NRC
5. document estimated HEAF ZOIs for an array of scenarios.

2 OVERVIEW OF MODEL AND IDENTIFICATION OF AREAS OF DISSIMILARITIES

2.1 Introduction

Modeling the hazards associated with electrical arc flashes has been ongoing since at least the early 1980's by the well-known work of Ralph Lee [12]. However, experience over time indicated that Lee's formulas didn't reconcile the greater thermal effect on persons positioned in front of open doors or removed covers [11]. Work by Doughty, Neal and Floyd identified the contribution of thermal energy from electrical enclosure interior surfaces. In 2002, the Institute of Electrical and Electronic Engineers (IEEE) published its initial model using new, empirically derived models based on statistical analysis and curve fitting of the overall test data. While the 2002 model has been used successfully, it was also recognized that not enough arc-flash incident energy testing had been done from which to develop models that accurately represent all of the real applications [13].

In 2018, the IEEE revises its model for performing arc-flash hazard calculations [11] (referred to as the "initial model" in this report). The revision to the base model was based on a multi-year, multi-million-dollar research program organized by IEEE and the National Fire Protection Association (NFPA) with support the industry vendors and organizations. The model documented uses over 1,860 tests to develop an empirical model based on statistical analysis and curve fitting. The number of configurations was expanded from two in the 2002 edition to five in the 2018 edition.

2.2 Initial Model Overview

The initial model estimates incident energy at a specified distance and the arc flash boundary for personal using electrical system characteristics as inputs. The initial model is applicable over a wide parameter range that covers the majority of the fire PRA scenarios [11]. The initial model is empirically derived based on statistical analysis and curve fitting to the overall test data available with the understanding of the underlying electrical arc physics. Based on these results, the initial model incident energy calculation is primarily dependent on arc current, duration, and distance. Bus gap has a smaller influence on incident energy than these three parameters. The initial model is linearly dependent on arc duration, and an inverse exponential relationship with distance. The reader should review the initial model documentation [11] for a full description of the model and an understanding of its development and use.

The subsequent sub-sections provide a description of the overall calculation process, inputs and outputs, assumptions and limitations. Where differences between the initial model and the needs for the NRC assessment exist, they are identified. Evaluation and resolution of those differences are contained in Section 3.

2.2.1 Calculation process

The process used to perform the calculation is presented in the initial model [11]. It involves collecting the model input parameters, followed by performing a number of iterative calculations of arcing current and incident energy to arrive at the final incident energy and arc flash boundary.

For the purposes of the NRC assessment, the calculation is the same, however, the process is different in several ways based on the information available and differences in targets damage levels. These differences are summarized below.

- The arc flash boundary is not needed

  o This is based on limits for sustaining injury to humans and not applicable to fire PRA targets such as electrical cables and bus duct enclosures. As discussed below the zone of influence (ZOI) will be determined using the HEAF PRA target fragility thresholds [14].

- Initial model uses bolted fault current, final model uses arcing fault current

  o Updated HEAF PRA scenarios (EPRI / U.S. NRC 2021) present arcing fault current and not bolted fault current. Bolted fault current are iteratively solved for convergence to the desired arcing fault current for the HEAF PRA scenario.

- The distance to target is not known.

  o The distance from the initiating source to the target is a desired output and not an input. The calculation will be solved iteratively to find the distance where the incident energy converges to the target fragility threshold. The distance where the hazard incident energy equals the target fragility threshold is then the zone of influence (ZOI) for the specific hazard scenario. Consistent with the guidance provided by the initial model, the modified model is not applicable for targets less than 0.3m (12 in.). As such, the user would have to consider targets within 0.3 m (12 in.) from the source to be within the ZOI.

- Additional modifications to the calculation are made to account for dissimilarities between the initial model assumptions and the PRA model assumptions, including insights from operational experience. The specific modifications are discussed in Section 3.4 and include;

  o Enclosure breach and opening delay

  o Model bias adjustment

  o Generator fed decay

2.2.2 Inputs

Several inputs are required, as described below.

Conductor Gap Spacing (G)
This is the gap distance between the electrodes. In most cases, acquiring this information may be difficult. However, several resources online are available to provide representative distances. For the evaluation of the initial model, the test data sets included this measurement.

Open Circuit Voltage (V_{oc})
This is the pre-fault voltage. For this input the actual system nominal voltage or utilization voltage can be used. Examples of nominal system voltage include 480V, 4.16kV, 6.9kV, 13.2kV, etc.

Arc Duration (T)
This is the total duration of the arc. The initial model does not identify an upper limit.

Distance (D)
The distance between the arc and the fire PRA target.

Bolted fault current
Determining the bolted fault current at the fault location requires detailed knowledge of the electrical distribution system design and set points. This information is not readily available to the staff. However, the fire PRA scenarios have identified or calculated the ranges of arcing fault current that were experienced during actual HEAF events (i.e., operational experience). The arc fault current is an output of the initial model. Therefore, the application of the final model has been adapted by performing a numerical iteration of the bolted fault current input to converge the calculated arcing current to the specified arcing fault current that matches the HEAF scenario.

Electrode configuration
The initial model provides five configurations to select. Two of the configurations are for open air, a third is for an insulated enclosure configuration (not insulated bus bars) that is not expected to be used. Therefore, three configurations are not considered applicable to the HEAF scenarios. The remaining two have applicability for the intended purposes and selection of a configuration will be dependent on the location of the arc and the orientation of the targets.

Enclosure Dimensions
The model requires the enclosure dimensions as input. This includes the width, height, and depth of the enclosure relative to the target. The model validation is limited by the size of compartments used in tests. If the volume of the enclosure exceeds the model limits in either direction, the input parameters should be adjusted to most accurately represent the zone of interest.

2.2.3 Model outputs

The model outputs include arcing fault current and incident energy.

Arc fault current
As discussed above, the information available to the staff has identified a range of arcing fault currents and as such, the bolted fault input is to be iteratively adjusted to match the calculated arc fault current with the expected arc fault current. This is easily performed in Microsoft Excel using the goal seek function.

Incident Energy
The model calculates the incident energy at the specified location based on the inputs. The incident energy is reported in units of MJ/m^2.

Zone of Influence
The zone of influence (ZOI) can be estimated by numerical iteration of the model by iterating the distance (D) where the incident energy matches the target fragility threshold. The NRC and EPRI joint working group has identified $15MJ/m^2$ and $30MJ/m^2$ for the targets of interest to fire PRA [14].

2.2.4 Assumptions

For the fire PRA application, the HEAF zone of influence is needed. This is the distance from the enclosure where targets are assumed to be damaged. Since the initial model doesn't

perform fire thermal dynamics, any target ignition and flame propagation beyond the initiating source (HEAF enclosure) is not included the application of the initial model. Therefore, the ensuring fire is not addressed in this report, but should be considered in the overall assessment of the HEAF hazard.

2.2.5 Limitations

The initial model specifies several limitations, these include

- Dimensions
    - o Limits on maximum enclosure dimensions with limit on opening area.
    - o Minimum width based on conductor gap spacing

3   EVALUATION

The purpose of this section is to present an evaluation of the initial model predictions along with parameter sensitivity. The evaluations use data acquired during the NRC testing program that is different from the data used to develop the initial model.

3.1   Evaluation Process

The initial model was evaluated against the NRC dataset followed the same process as used in the NRC/EPRI fire model validation found in NUREG-1824 [16]. This approach involves a scatter plot consisting of the experimental (measured) values represented by the horizontal axis and the model (predicted) values represented by the vertical axis. If a particular prediction and measurement are the same, the resulting point falls on the solid diagonal line. To better make use of these results, two statistical parameters are calculated for each model and each predicted quantity. The first parameter, δ, is the *bias factor*. It indicates the extent to which the model, on average, under- or over-predicts the measurements of a given quantity. For example, if the bias factor is 1.10, this indicates that on average the model overpredict by 10%. The second parameter is the *relative standard deviation* of the model, $\tilde{\sigma}_m$. This indicates the variability of the model. In addition, the relative standard deviation of the experimental measurements is presented as $\tilde{\sigma}_e$. The degree of model uncertainty is indicated by the extent to which the data scatter outside the experimental bounds. The calculation of bias and relative standard deviations was performed in Microsoft Excel™.

3.2   Overview of data

Two sets of data are used for evaluation. A series of tests performed on medium-voltage switchgear performed in 2018 [16], and a series of simple open box configurations performed 2019 at medium-voltages [17]. The open box data provides a convenient evaluation of the initial model as they are of a configuration like those used to develop the initial model (vertical closed box). The 2018 switchgear provides valuable reference as to the event evolution in full-scale equipment. The data summary is presented in Table 1 and Table 2. Photos of experimental configuration is shown in Figure 1 and Figure 2.

Table 1. Summary of open box tests

Test	Electrode Material	System Voltage (kV)	Current (kA)	Duration (s)
OBMV01	Aluminum	6.9	14.3	3.18
OBMV02	Aluminum	6.9	29.1	1.12
OBMV03	Aluminum	6.9	14.4	5.05
OBMV04	Copper	6.9	14.3	5.08
OBMV05	Copper	6.9	28.6	2.32
OBMV06	Aluminum	6.9	14.6	2.05
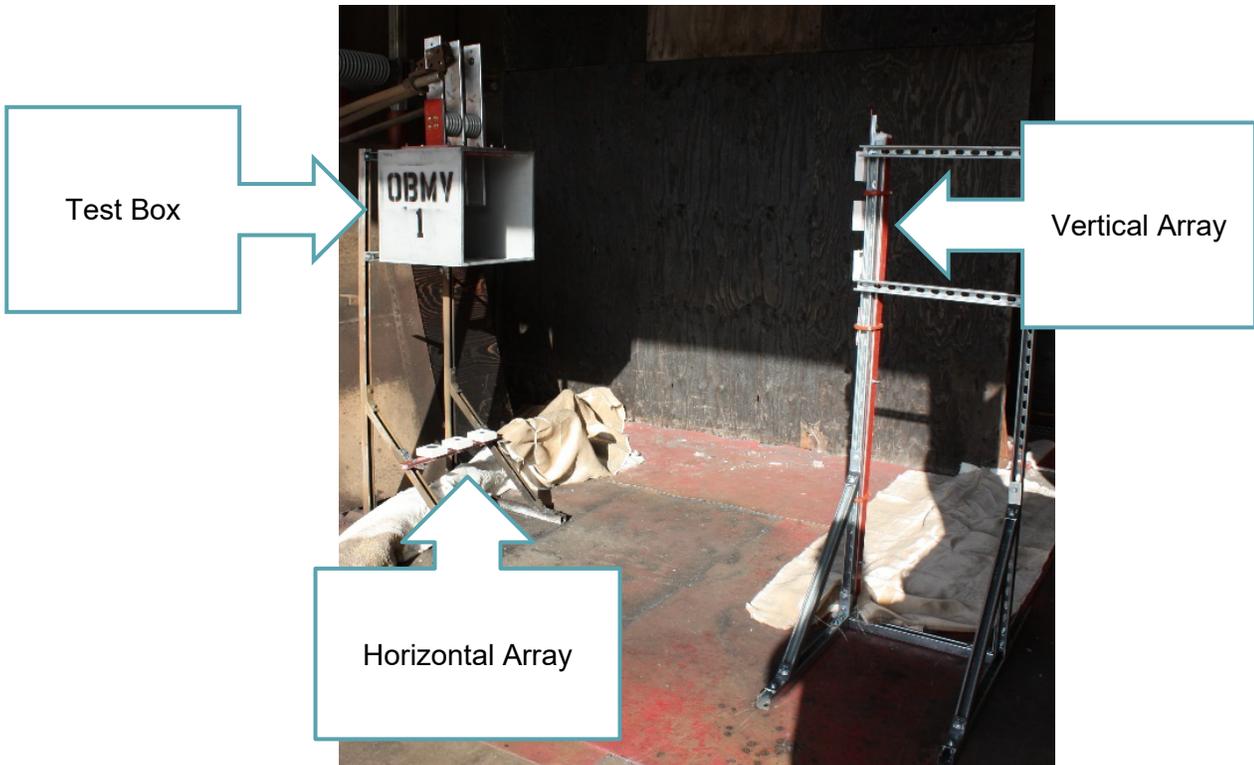
Figure 1. Open box medium-voltage test configuration. Vertical sensor array (right), Horizontal sensor array (bottom left)
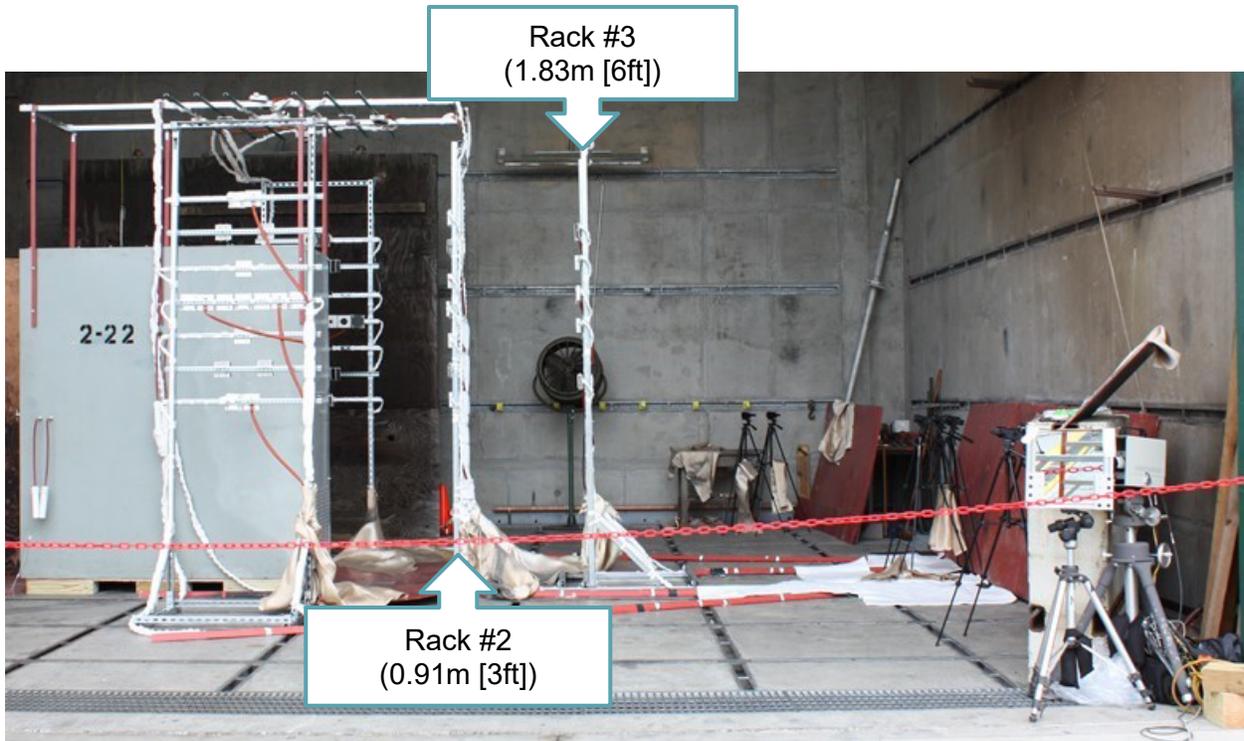
Figure 2. Medium-voltage Switchgear Test Configuration (Test device shown at left, Instrument Racks #2 and #3 used for evaluation)

Test	Electrode Material	Voltage (kV)	Current (kA)	Duration (s)
2-19	Aluminum	6.9	25.8	2.0
2-21	Aluminum	6.9	26.6	4.1
2-22	Aluminum	7.0	32.0	2.1
2-24	Aluminum	7.0	29.8	4.2

* Voltage was only measured at Generator and is not the same as arc voltage.

3.3 Initial model evaluation

The initial model [11] is first evaluated against the NRC data without any modification. The two data sets were evaluated separately due to the differences in the experimental configuration. The comparison uses incident energy in units of MJ/m^2. This is one of the outputs of the model and is used to characterize target fragility.

The vertical closed box configuration in the initial model represents the open box test configuration. The model comparison to the open box test data is presented in Figure 3 and shows a model underprediction of 32% (Bias = 0.68).
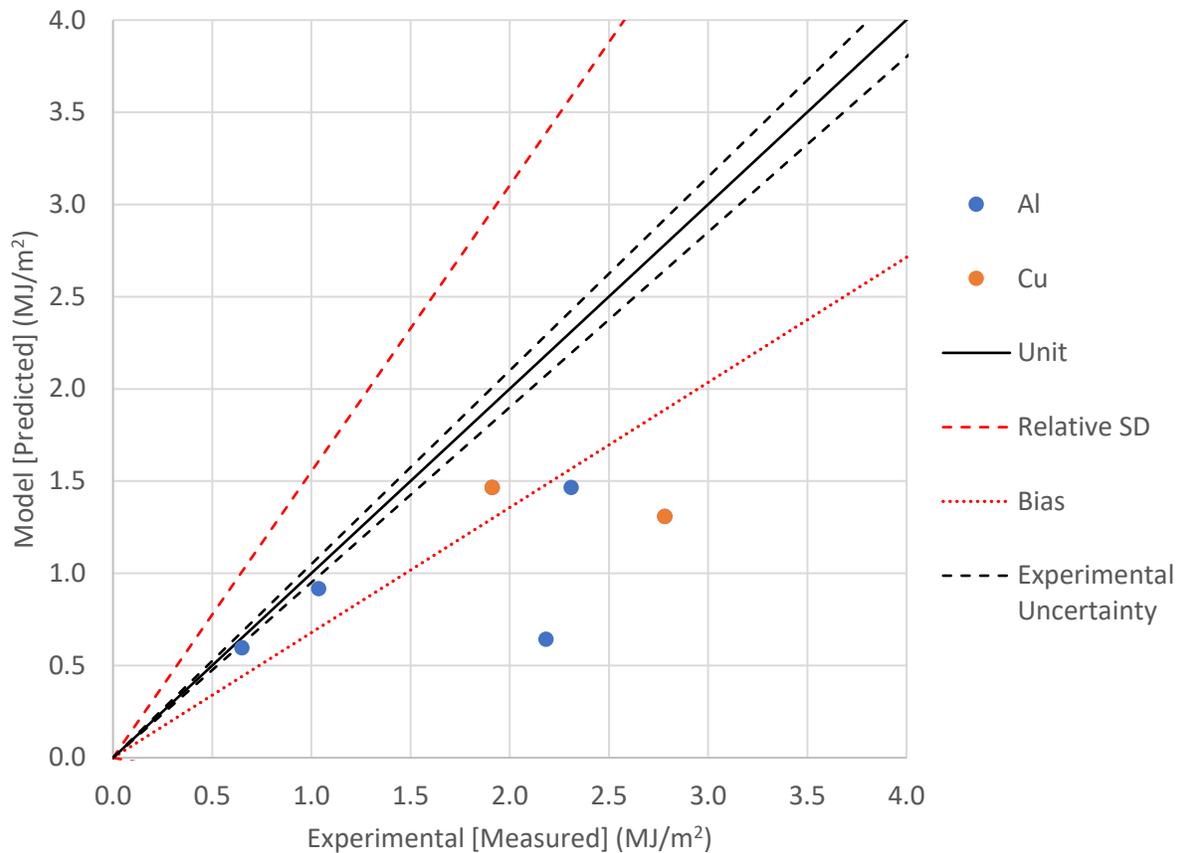
Figure 3. Open Box - Initial Model VCB (Bias = 0.68; SD_M = 0.44) Al – blue, Cu - orange

Next the initial model was used to evaluate the medium-voltage switchgear results. The switchgear test comparison showed a 133% overprediction as shown in Figure 4. Since the configuration was different than the model assumptions this overprediction was expected. However, it was also noted that the data sets were segregated by test duration. Splitting the data sets up by duration 2 second vs 4 seconds and re-evaluating the model to each data set indicated a 256% overprediction for the short duration tests and a 7% underprediction for the longer 4 second duration tests. These results are presented in Figure 5 with photographs of the post-test equipment shown in Figure 6 and Figure 7.
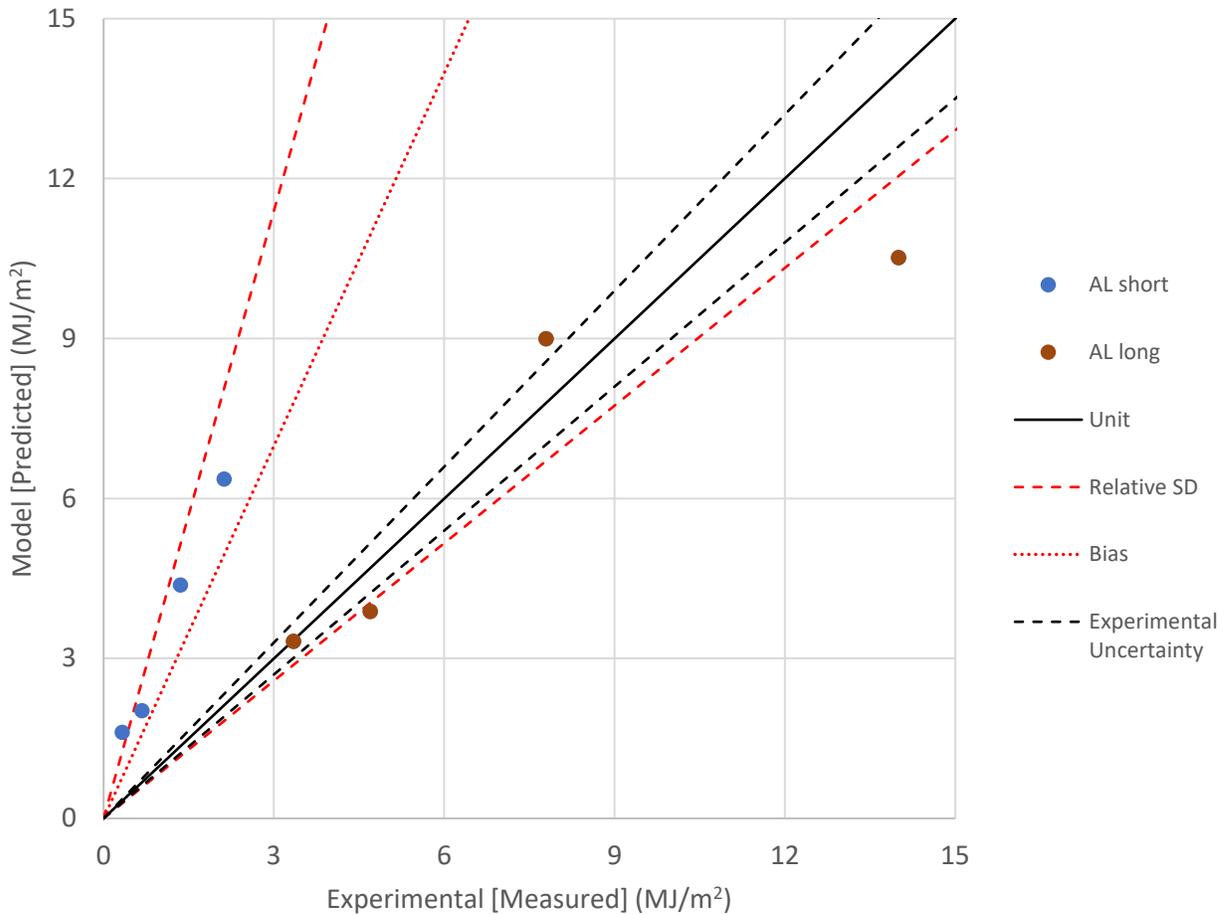
Figure 4. Switchgear MV - Initial Model, short duration blue, long duration red (Bias = 2.33; SD_M = 0.74) [Blue : 2 sec; Red : 4 sec]
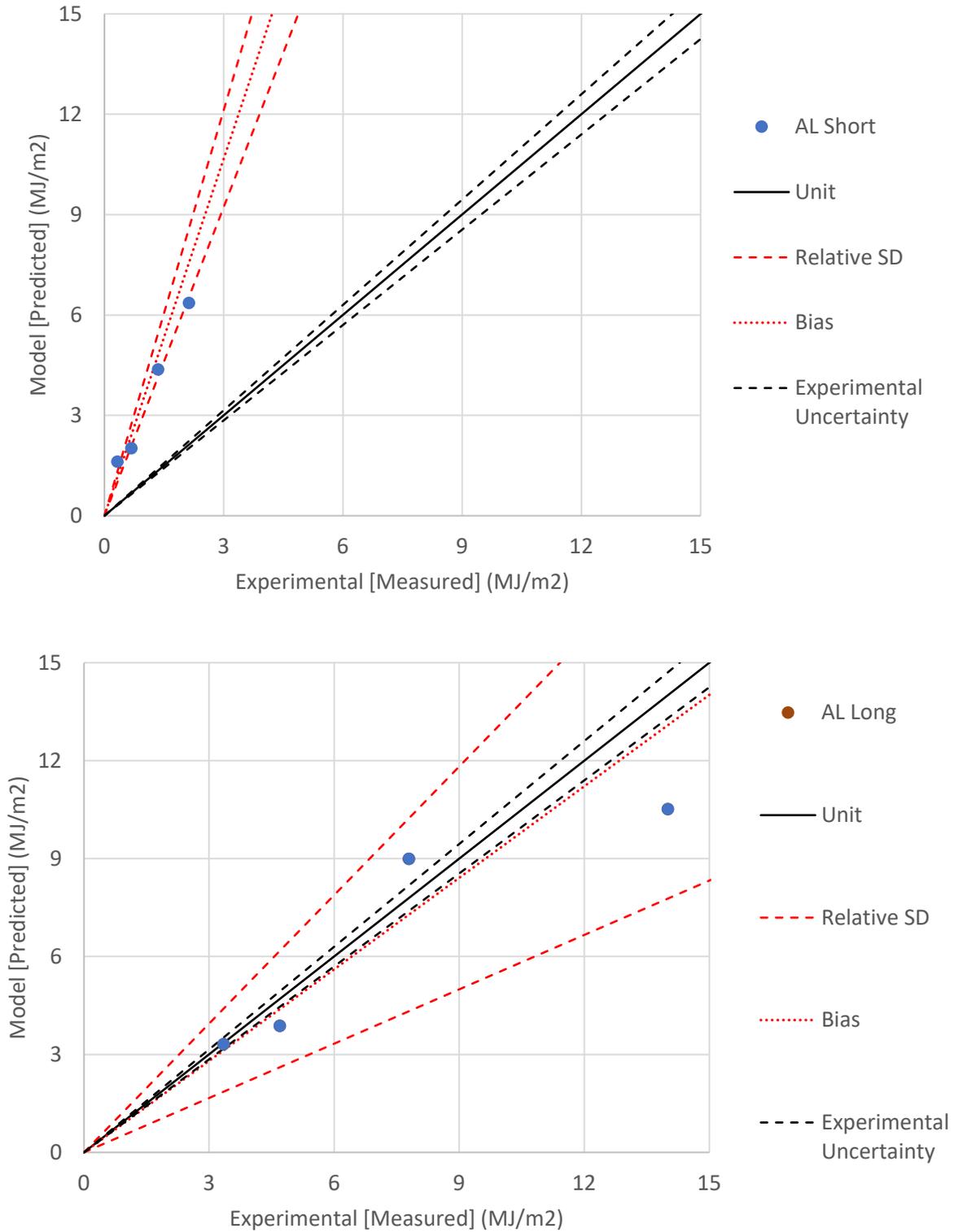
Figure 5. Switchgear MV - Initial Model by Duration. Top - 2 seconds overprediction (Bias = 3.56; SD_M=0.24); Bottom - 4 seconds underprediction (Bias = 0.93; SD_M=0.19)

Figure 6. Photographs of 2 sec test enclosures (Left 2-19 25.8kA 39MJ / Right 2-22 32.0kA 51MJ)

**Figure 7. Photographs of 4 sec test enclosure (Left 2-21 26.6kA 101MJ /
Right 2-24 29.8kA 122MJ)**

As can be seen by Figure 5 the short duration tests group differently from the longer 4 second duration. Observations of the video data suggest that the difference can be due to the amount of time the calorimeters are exposed to the arc energy. In the short duration tests a larger fraction of the test duration involves the heating up, melting and yielding of the steel enclosure. Since the initial model assumes direct exposure to the arc energy, the time required to create an opening in the steel enclosure needs to be estimated to arrive at a more accurate exposure time for incident energy calculations. Subsequent sections present the modification to the model to better align with fire PRA scenarios and assumptions.

3.4   Breach modification evaluation

One difference between the initial model and the fire PRA scenarios (including test data) is that the initial model assumes no barrier between the source and the target. However, in U.S. events, it is common for the event to occur with the enclosure under fault in the closed condition (no open doors or panels). While exceptions do occur, this analysis assumes that the enclosure is closed. This assumption results in the need for the energy from the HEAF to be absorbed by the electrical enclosure to cause breach, resulting in an initial energy to be lost to the enclosure and not transmitted to the external targets. This evolution effectively results in a shorter time duration for the exposure of external targets. Therefore, if the time to breach and time to create

an enclosure opening sufficiently large enough to effectively transfer heat to targets can be estimated, this time can be used to offset the time used in the initial model. The initial model is linearly dependent on time, and therefore time can be modified as proposed below. In Figure 8, the arc duration is the same as the fault duration. It is decomposed in to three components; time to breach, time for breach to expand to effectively transfer energy outside the enclosure and the target exposure time.
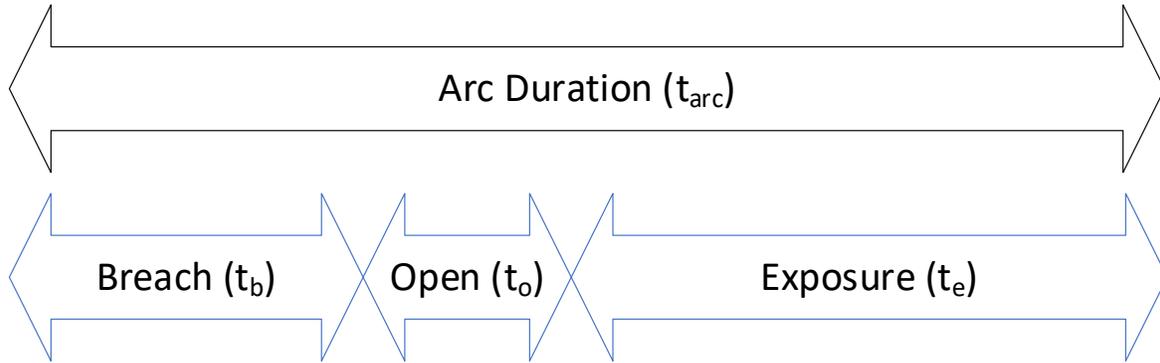
Figure 8. Illustration of Arc timeline (Not to Scale)

$$t_e = t_{arc} - t_b - t_o \tag{1}$$

Where, t_e, exposure time
t_{arc}, arc time [PRA scenario estimate]
t_{ib}, time to initial breach enclosure
t_o, time to open from initial breach

The exposure time represents the time that the external targets are exposed to the HEAF. This is calculated by subtracting the time to the initial breach and the time from initial breach to sufficient opening from the arc time. These two quantities are estimated as described next to reach the final form shown below. Note that the basis for this equation is developed in subsequent sections (3.4.1 and 3.4.2)

$$t_e = t_{arc} - t_b - t_o = t_{arc} - \frac{k}{\delta} \frac{h^2}{I_{arc}} \cdot 10^{-3} - \frac{\xi \cdot \theta}{V_{arc(L-L)} I_{arc}} \tag{2}$$

Where,

k(steel) = 2,434   k(aluminum) = 566
δ = 0.9   Iarc, arc current (kA)
h, enclosure thickness (mm) t_b, breach time (s)
Varc(L-L), arc voltage Line-to-Line (kV)   θ, material parameter (1 steel, 0.25 aluminum)
ξ, configuration factor (3.9 Switchgear, 1.2 bus duct)

3.4.1 Time to initial breach (t_b)

The time to breach (t_b) represents the time from the arc initiation (t=0) to the time when the enclosure starts to breach. The literature was reviewed and found existing models to predict the time to breach of an enclosure. Most of the literature found was related to gas insulated substations (GIS) [19, 20, 21, 22, 23]. These models follow the following general form:

$$t_b = k \frac{h^\alpha}{I^\beta} \tag{3}$$

Where k is a material dependent parameter, h is the enclosure thickness, I is the current, and α and β are model fitting parameters proposed by the authors. Evaluation of these models against NRC data indicated a large underprediction (63%) in the time to breach, which would cause a conservative estimate on the time to exposure. Further evaluation of these models identified that the geometrical differences between the GIS system and a flat panel system such as HEAF equipment may be causing the model bias. The GIS systems use a cylindrical housing with the conductor in the center versus the switchgear or bus duct enclosures that are made of flat panels. Modification of the material dependent parameter by π (to account for geometric differences) brought the model predictions into better alignment (10% underprediction) as shown in Figure 9.
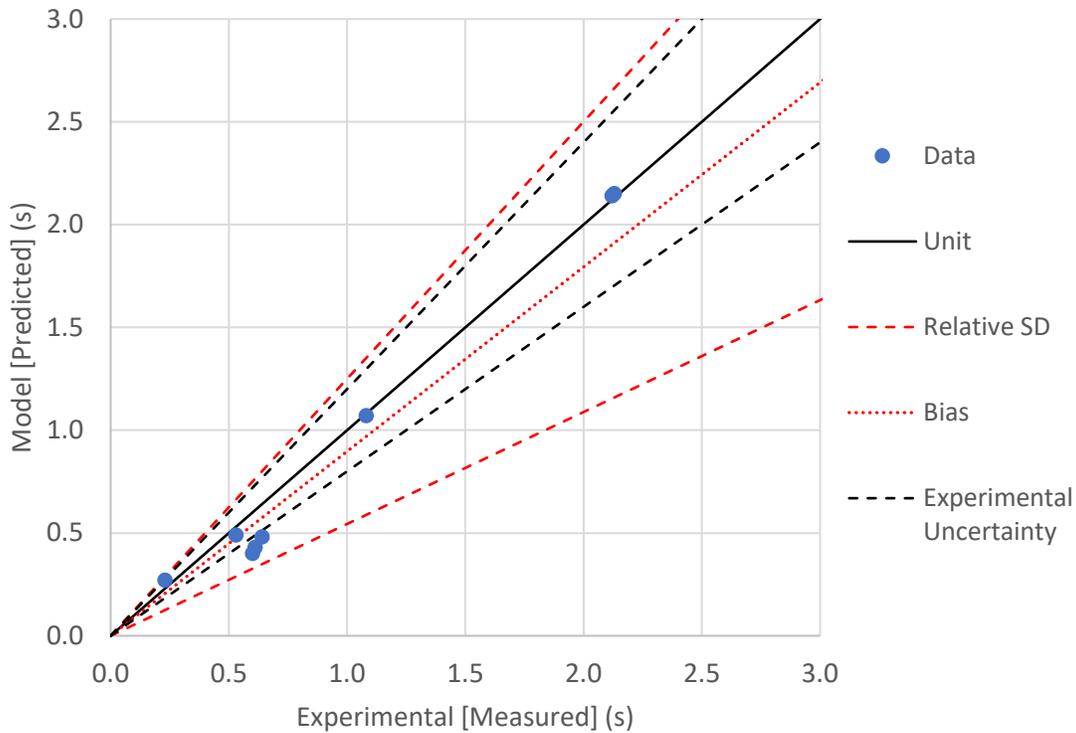
Figure 9. Modified burn-through steel enclosure (Bias = 0.90, SD_M = 0.18)

The equation presented above also suggests the difference between the burn through time is approximately 4.3 times longer for a steel enclosure versus an aluminum enclosure of the same thickness and arc current. Similar results were derived during the NRC fragility evaluation [14].

Therefore, the time to initial breach (t_b) is calculated as follows,

$$t_b = \frac{k}{\delta}\frac{h^2}{I}$$

(4)

k(steel) = 2,434
k(aluminum) = 566
δ = 0.9
I, arc current (kA)
h, enclosure thickness (mm)
t_b, breach time (ms)

3.4.2 Time to open from initial breach (t_o)

Evidence from high speed videography indicates that the opening starts small and expands as more energy is used to melt or yield the metal enclosure. The mass loss of the enclosure can be estimated based on pre- and post- test measurements. However, the limited amount of mass loss compared to the total mass of the enclosure excluded the ability to take a time resolved mass loss measurement during test.

The total enclosure mass loss versus total estimated energy for the 2018 medium-voltage switchgear experiments [16] is presented in Figure 10. Similar linearity with energy is found from the open box test data [17] shown in Figure 11, including a notable difference between steel mass loss dependent on electrode material (copper or aluminum). It is also noted that the full scale 2018 data shows a lower mass loss per electrical energy input. This is likely due to configuration differences (larger volume space in 2018 full scale). As such, the full-scale results are used to estimate an opening area for switchgear and the smaller scale box tests used to estimate the opening area for bus ducts.
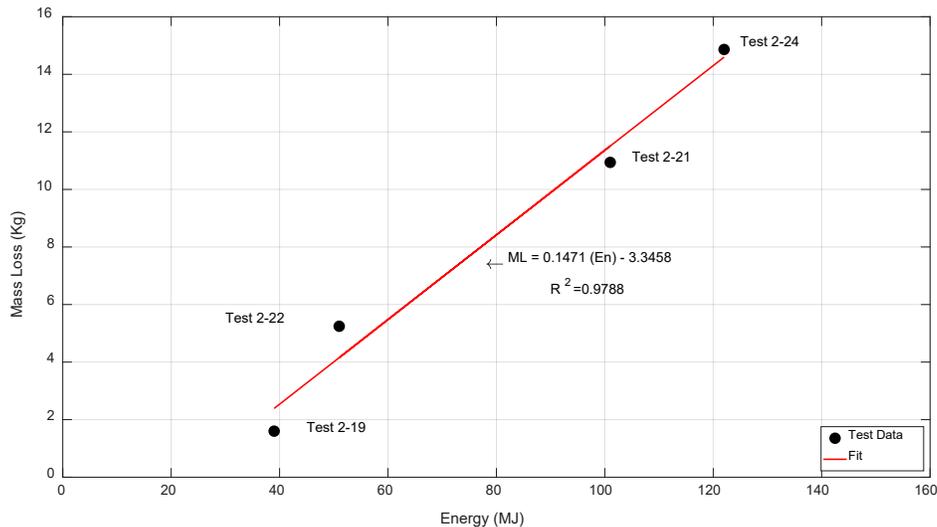
Figure 10. Steel enclosure mass loss versus electrical energy with aluminum bus bars (2018 arc energy estimated)
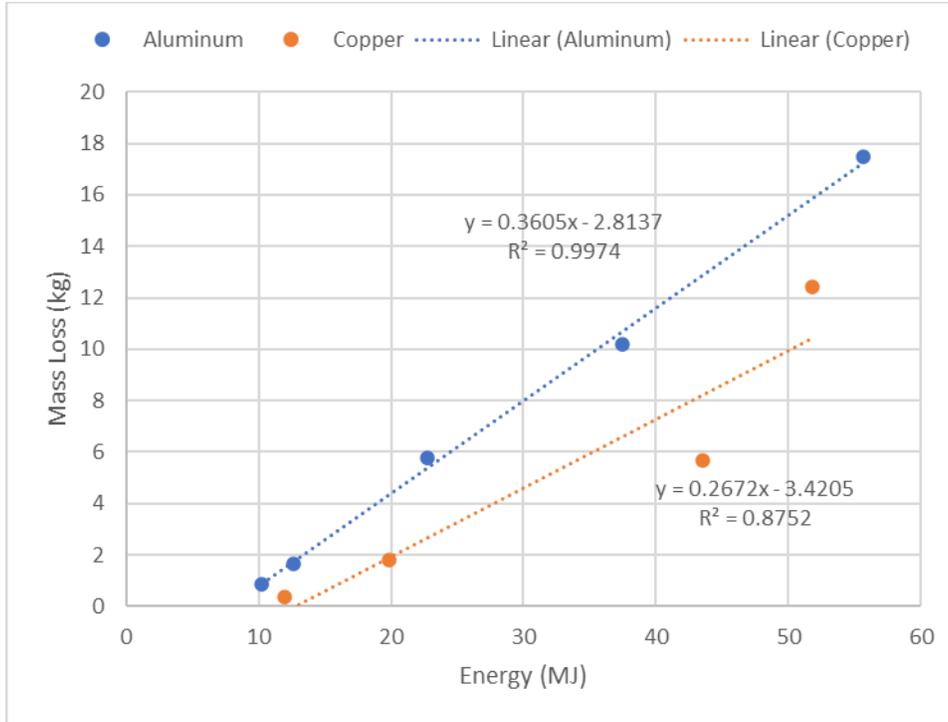
Figure 11. Steel enclosure mass loss versus arc energy (with aluminum or copper bus bars)

Based on a review of the medium-voltage switchgear data and high speed video, the size of the opening between initial breach and efficient energy transfer to targets external to the enclosure was approximated at 550 cm^2 (85 in^2), which correlates to a mass loss of 0.99 kg and 6.75 MJ of energy for the 2018 tests. Therefore, the time to open from breach is estimated as,

$$t_o = \frac{Energy\ to\ open}{Power}\ [s] \tag{5}$$

For a PRA scenario, the arc power needs to be calculated using the following form:

For Medium-voltage:

$$\text{Arc power} = \sqrt{3}*(V_{L\text{-}L})*I = \sqrt{3}*(V_{arc(L\text{-}L)})*(I_{arc})*(1E\text{-}6)\ [MJ] \tag{6}$$

For Low-voltage:

$$\text{Arc power} = \sqrt{3}*(V_{L\text{-}L})*I = \sqrt{3}*(V_{arc(L\text{-}L)})*(I_{arc})*(1E\text{-}6)\ [MJ] \tag{7}$$

Therefore,

$$t_0 = \frac{3.9*\theta}{V_{arc(L-L)}I_{arc}\cdot10^{-6}}\ [s, SWGR] \tag{8}$$

Where θ is 1 for Steel and 0.25 for aluminum enclosures and $V_{arc(L\text{-}L)}$ is 650$V_{L\text{-}L}$ for Medium-voltage and 350$V_{L\text{-}L}$ for low-voltage. See Appendix A for selection of arc voltage.

The analysis above was done using the MV switchgear data that is applicable for larger volume enclosures. For smaller non-segregated phase bus ducts, the medium-voltage box tests appear to be more appliable for the geometry. For the medium-voltage box tests, the same analysis of the data and high-speed video was performed. The corresponding mass loss 0.77kg or 2.14 MJ of energy, which results in a breach to open time (t_0) of,

$$t_0 = \frac{1.2 * \theta}{V_{arc(L-L)} I_{arc} \cdot 10^{-6}} \; [s, bus \; ducts] \tag{9}$$

Where θ is 1 for Steel and 0.25 for aluminum enclosures and $V_{arc(L-L)}$ is 650V_{L-L} for Medium-voltage and 375V_{L-L} for low-voltage.

3.5   Model breach and open time evaluation

Similar to what was done in Section 3.3 the model predictions will be evaluated against experimental data using the exposure time rather than the arc time. These results are presented below.
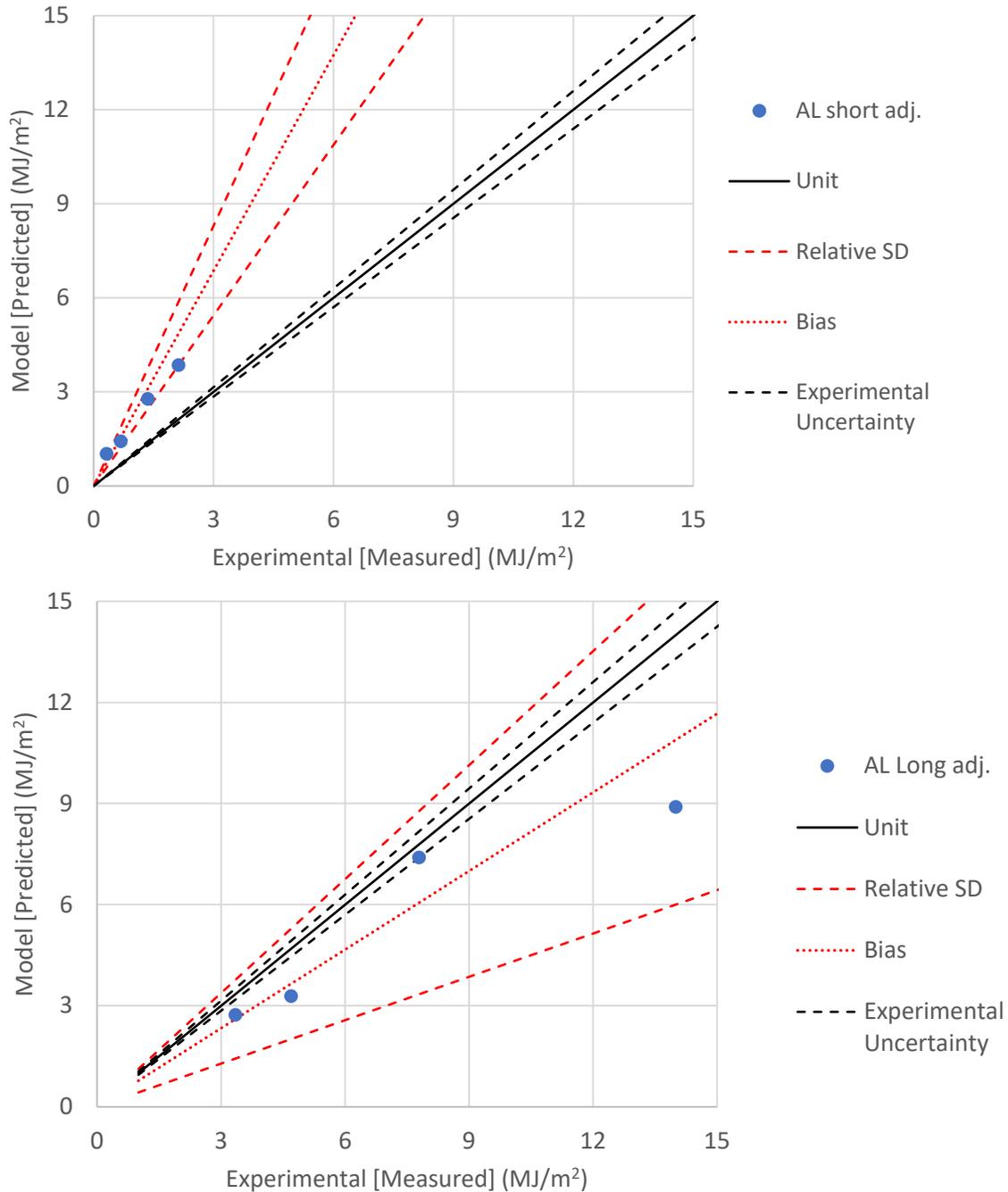
Figure 12. Switchgear MV – Breach Modification Model by Duration. Top - 2 seconds overprediction (Bias = 2.29; SD_M=0.24); Bottom - 4 seconds underprediction (Bias = 0.78; SD_M=0.17)
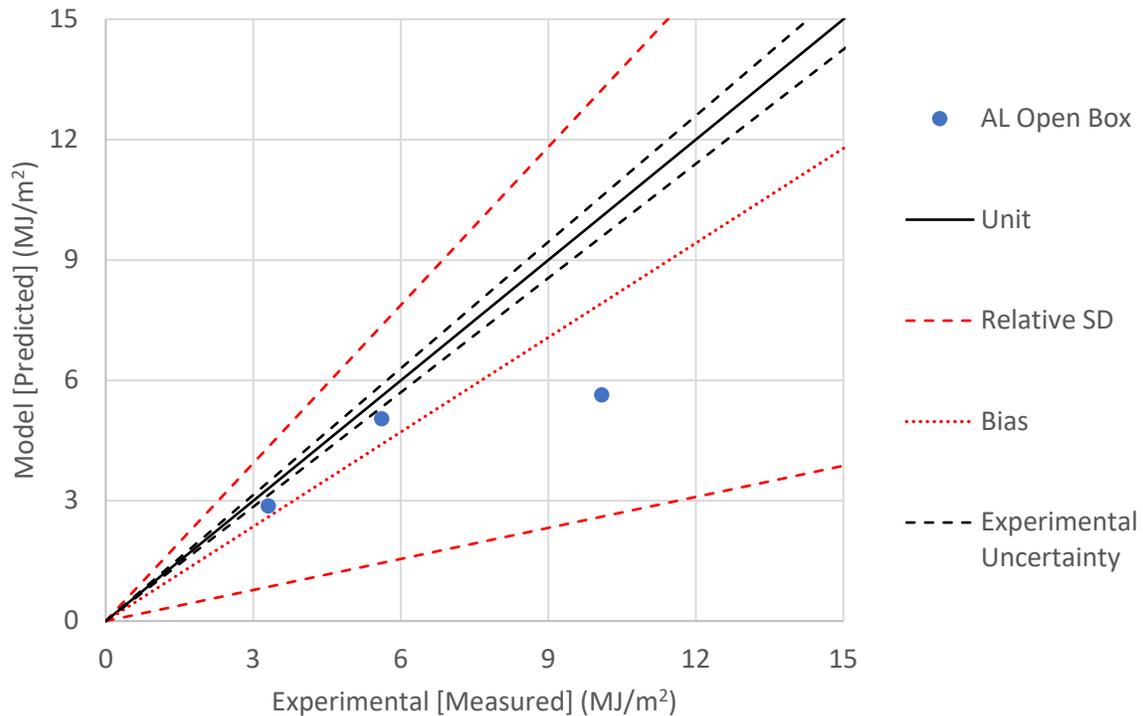
Figure 13. Open Box MV – Breach Modification Model by Duration (note OBMV05 did not breach). (Bias = 0.79; SD_M=0.26)

3.6   Generator fed – energy conservation modification evaluation

Generator fed faults on a unit connected design (no generator circuit breaker) have been identified as a leading contributor to long duration HEAFs [24]. Based on this, the NRC-RES contracted with CESI to develop a decrement energy curve based on a typical nuclear power plant design and reference data from an event occurring at a U.S. facility. This effort resulted in developing a power decay curve shown in Figure 14.
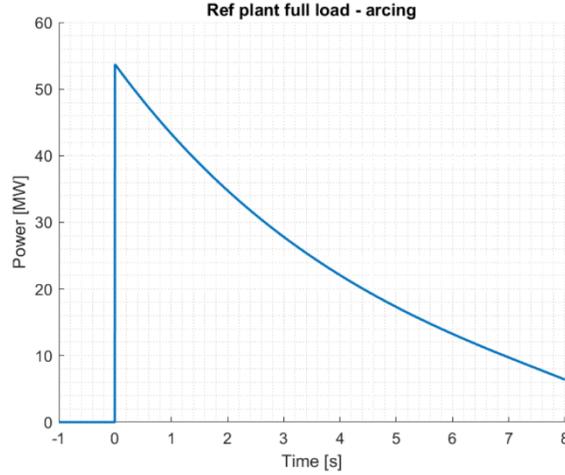
Figure 14. Reference plant decrement curve

From this work, the arcing current is defined as,

$$i_t = I_t e^{\frac{-t}{T'_{ref}}}$$ (10)

Where,　　T'$_{ref}$ = 4.75
　　　　　I$_t$, initial arcing fault current (kA)
　　　　　t, time (seconds)
　　　　　i$_t$, decaying arcing fault current (kA)

The development of this curve is based on plant operational event data provided to the NRC-RES via a collaborative research agreement (Memorandum of Understanding). A subsequent event that occurred in December 2020 has provided additional insights and suggests that the current decay time constant (T'$_{ref}$) may be larger. The time constant is dependent on the plant equipment characteristics and as such all events will have a slightly different time constant. For the evaluation presented below, the CESI value is used and as such, may result in non-conservative estimates, if the final agreed upon time constant is larger than 4.75.

Arcing power can be determined as,

$$P_t = \sqrt{3} * V_{arc}^{LL} * i_t$$ (11)

where,　　P$_t$, decaying arc power (MW)
　　　　　V$_{arc}^{LL}$, arc voltage (kV) [see Appendix A for discussion on arc voltage]
　　　　　i$_t$, decaying arcing fault current (kA)

and arc energy,

$$E_t = \int_0^t P_t \, dt = \sqrt{3} \cdot V_{arc}^{LL} \cdot I_t \int_0^t e^{\frac{-t}{T'_{ref}}} \, dt = \sqrt{3} \cdot V_{arc}^{LL} \cdot I_t \cdot T'_{ref} \left[1 - e^{\frac{-t}{T'_{ref}}} \right]$$ (12)

Since the initial model was not built to input a decaying current profile, two approaches for conserving energy of the decrement curve but discretizing a constant power (i.e., current) for the initial model are proposed. The first approach is to adjust the time parameter in the initial model while maintaining the initial fault current (I_T) constant. Since the model output (incident energy) has a linear dependency with time this approach appears reasonable. Therefore, the model energy is equated to the arc energy and solved for the model duration (t_m) using the scenario duration (t_s) as shown below, with results of the constant current approach presented in Table 3.

$$t_m = T'_{ref} \left[1 - e^{\frac{-t_s}{T'_{ref}}} \right] \tag{13}$$

Table 3. PRA scenario time to Model Time for Decrement Scenarios

Scenario Time (t) [seconds]	Model Time (t_m) [seconds]	Scenario Time (t) [seconds]	Model Time (t_m) [seconds]
1	0.9	9	4.0
2	1.6	10	4.2
3	2.2	11	4.3
4	2.7	12	4.4
5	3.1	13	4.4
6	3.4	14	4.5
7	3.7	15	4.5
8	3.9		

The second approach is to maintain the same duration but adjust the fault current such that the total energy is conserved. This is illustrated in Figure 15, with results are presented in Table 4 using a 32kA base case (i.e., I_T = 32kA).
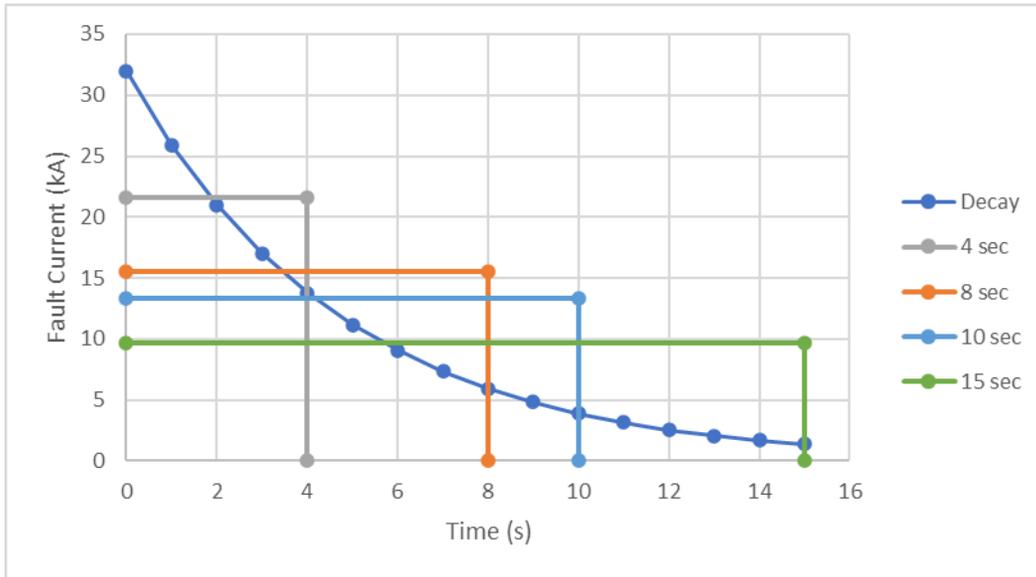
Figure 15. Example of constant time approximation showing current level and corresponding duration for select cases based on 32kA base Decay curve

Table 4. Constant duration decrement current modification based on an initial decay current of 32kA (I_T = 32kA)

Duration [seconds]	Current [seconds]		Duration [seconds]	Current [seconds]
4	21.6		10	13.3
5	19.8		11	12.5
6	18.2		12	11.7
7	16.7		13	10.9
8	15.5		14	10.3
9	14.3		15	9.7

These two approaches were compared using the modified model prediction of incident energy at three feet. The results are presented in Figure 16. The results indicate that the constant current approach using the base scenario case current (I_T) shows a slightly higher prediction. Without data to baseline the modification approach, the constant current approach using the initial fault current and a modified duration is suggested to reduce the likelihood of underprediction.
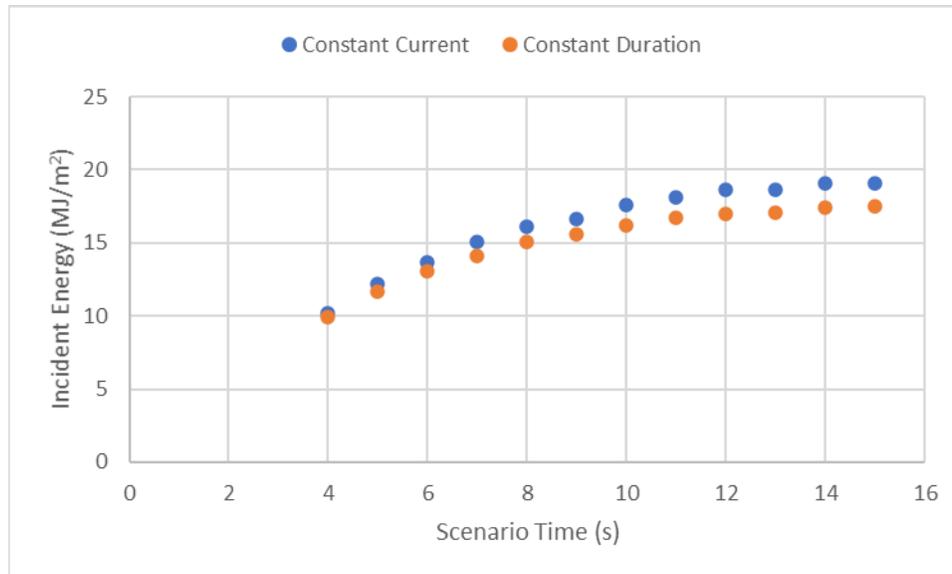
Figure 16. Comparison of Decay Curve Discretizing Approaches

3.7   Model Sensitivities and Model Evaluation Summary

The modified model requires several inputs to perform its calculation. This section evaluates the sensitivity of the modified model to each input, holding other inputs constant. The base scenario is as follows:

Parameter	Value		Parameter	Value
Voltage	6.9 kV		Configuration	HCB
Arc Current	28.5 kA		Duration	Variable (4 – 15s)
Gap Spacing	5.75 in		Enclosure	36 in x 36 in x 36 in (WxHxD)
Target Crit. IE	15 MJ/m^2		Enclosure Thickness	0.09 in
Enclosure Material	Steel		Enclosure Zone	MV Switchgear

The results are presented as plots of zone of influence (ZOI) versus duration. Since it is known that duration is linearly proportional to the incident energy calculated, this was chosen to be the dependent variable plotted on the horizontal x-axis. The results are presented in Figure 18. The range of parameter variation was based on information from operating experience, judgement, or model limitations. The ranges for each are described below.

Current: A low value of 23kA and a high value of 32kA was based on operational experience review of actual HEAF events.

Voltage: Medium-voltage was evaluated by selecting a common lower and higher medium-voltage level (4.16kV and 13.8kV).

Gap Spacing: Equipment manufactures, and other organizations have published typical bus bar spacing ranges for voltage level and equipment types. Based on this literature, a lower spacing of 10.2 cm (4 in) was based on the upper range of 5kV equipment, the difference between the

upper range of 5kV and 15kV equipment or 4.5 cm (1.75 in) above the base case resulted in the upper value of 19 cm (7.5 in).

Volume: The lower and upper limits were based on symmetry around the base value and the model limitations. All volumes were cubical in geometry. Thus, 61 cm (24 in) and 122 cm (48 in) square dimensions were used for the sensitivities.

Configuration: As noted previously the initial model has 5 configurations, 2 of which have the most applicability to the typical scenarios encountered. The HCB configuration involves the targets being aligned axially with the conductors. Arc behavior extends the arc plasms axially and as such HCB configurations experience higher incident energy when compared similarly to VCB. In the VCB configuration, the targets are perpendicular to the conductor axis. Since HCB provides the largest predicted exposure, it will be used for the sensitivity study. In practice the configuration that is most applicable to the equipment is selected. For equipment that has applicable to both configurations, the HCB is used to limit non-conservatism. Appendix B should be referenced for actual configurations used to develop the ZOI tables.

As expected, the results indicated that the model is most sensitive to the duration and current inputs. The current variations indicted a 9-13% increase or decrease in the zone of influence over the base case. The conductor gap spacing showed minimal variation with different gap spacings with maximum variations of 4-6%. System voltage was near identical for 4.16kV and 6.9kV, however the 13.8kV did show a minimal increase over the former two levels by approximately 6-7%. Volume also showed minimal change between the base case and a larger enclosure (1-3%) but did show a slight increase in the smaller volume enclosure of 6-9%.

As a final comparison, the VCB configuration was run and compared to the HCB configuration using the base case parameters. These results are shown in Figure 17 and show that the VCB ZOI differs from the HCB by approximately 30%.
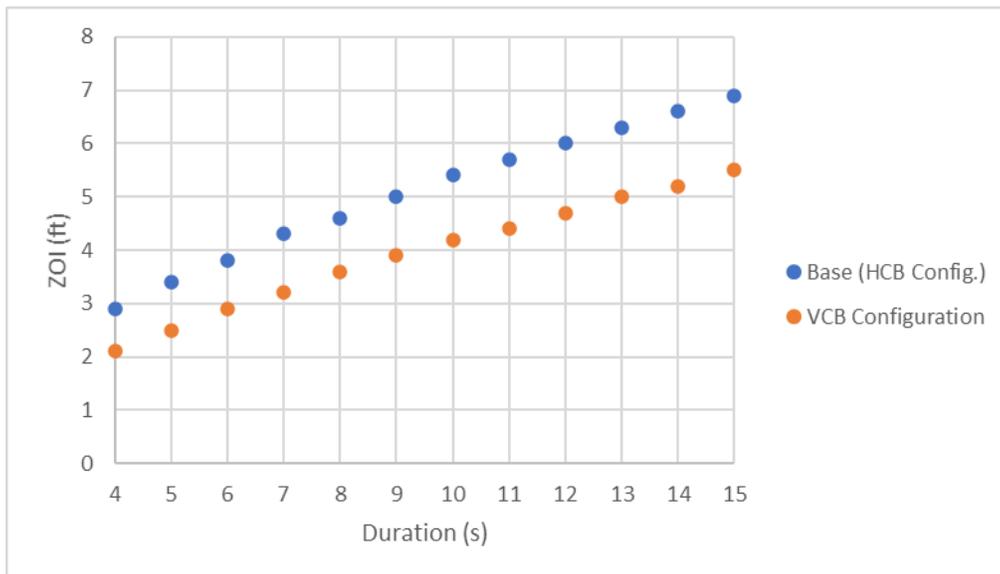
Figure 17. Base Case comparison between HCB and VCB

Table 5 presents a summary of the model comparisons discussed previously. For the ZOI developed later in this report, a bias correction factor of 0.78 was used. This was chosen for its applicability to the range of arcing durations evaluated and the similarity between the 4 second medium voltage switchgear and open box data.

Table 5. Summary of Bias and Relative Standard Deviation

Data Set	Bias (δ)	Relative Standard Deviation (σ)
Open Box MV - Base Arc Flash Model, VCB config.	0.68	0.44
MV Switchgear – Base Arc Flash Model, HCB config.	2.33	0.74
MV Switchgear – Base Arc Flash Model, HCB config. (2 second tests only)	3.56	0.24
MV Switchgear – Base Arc Flash Model, HCB config. (4 second tests only)	0.93	0.19
Modified Burn through model	0.9	0.18
MV Switchgear – Modified Arc Flash Model Breach and Open. (2 second tests only)	2.29	0.24
MV Switchgear – Modified Arc Flash Model Breach and Open. (4 second tests only)	0.78	0.17
Open Box MV – Modified Arc Flash Model Breach and Open	0.79	0.26
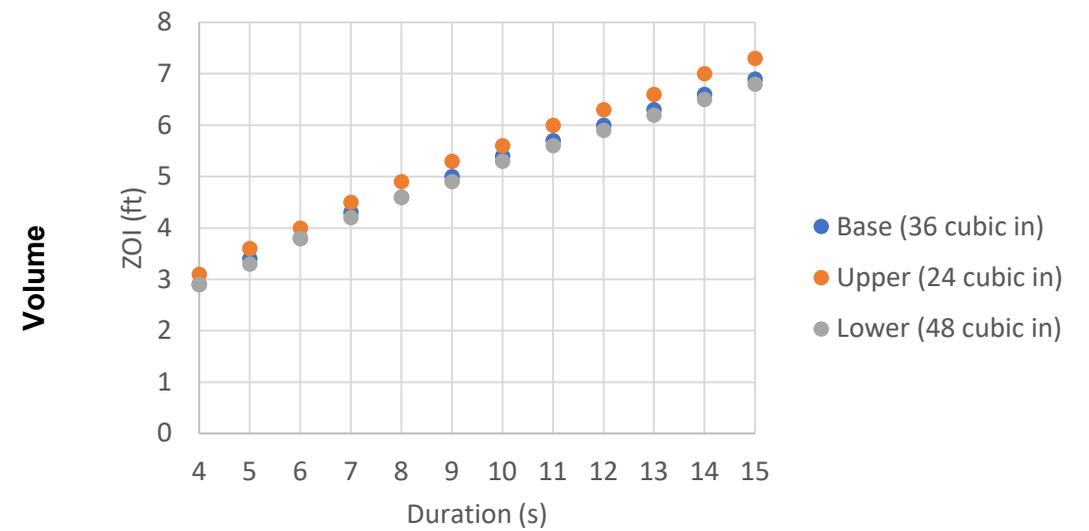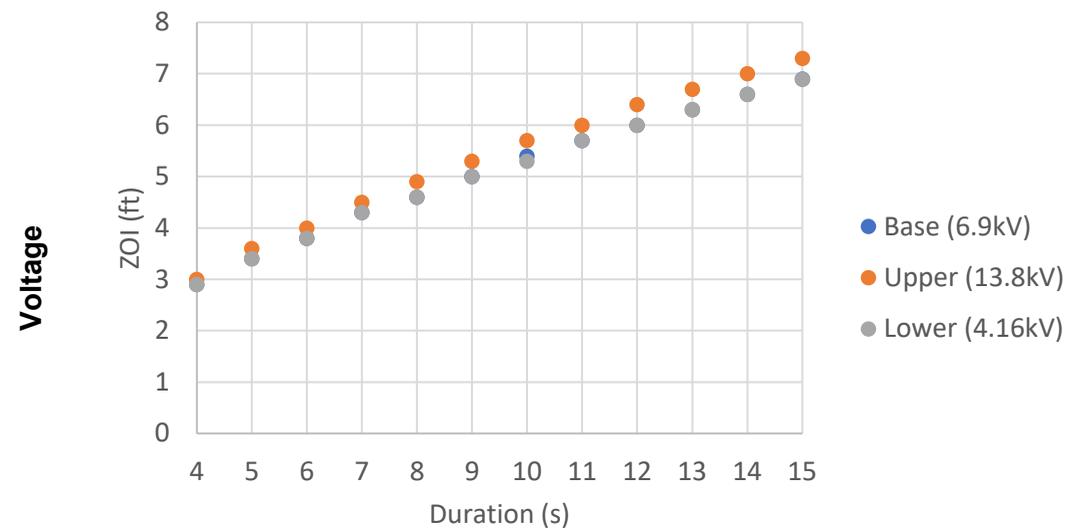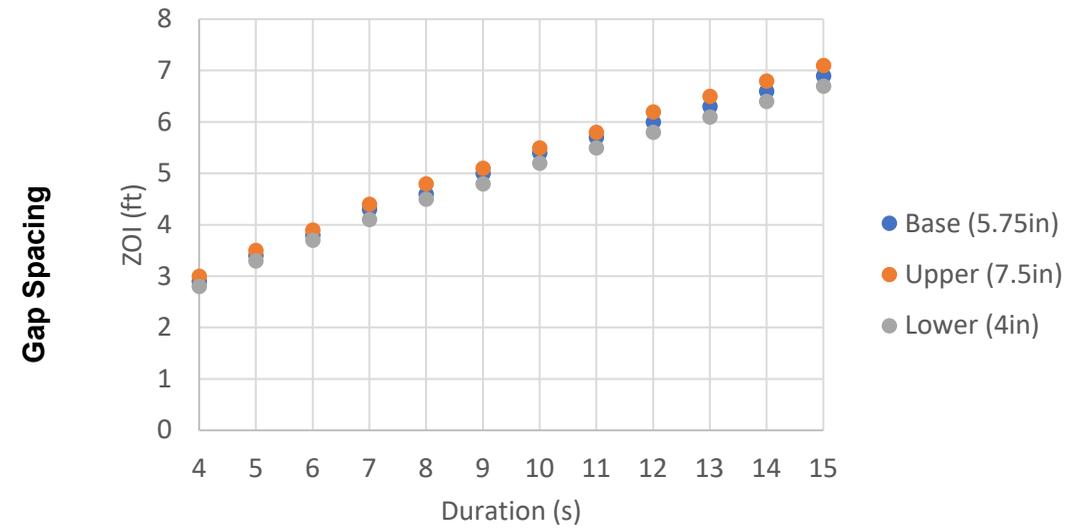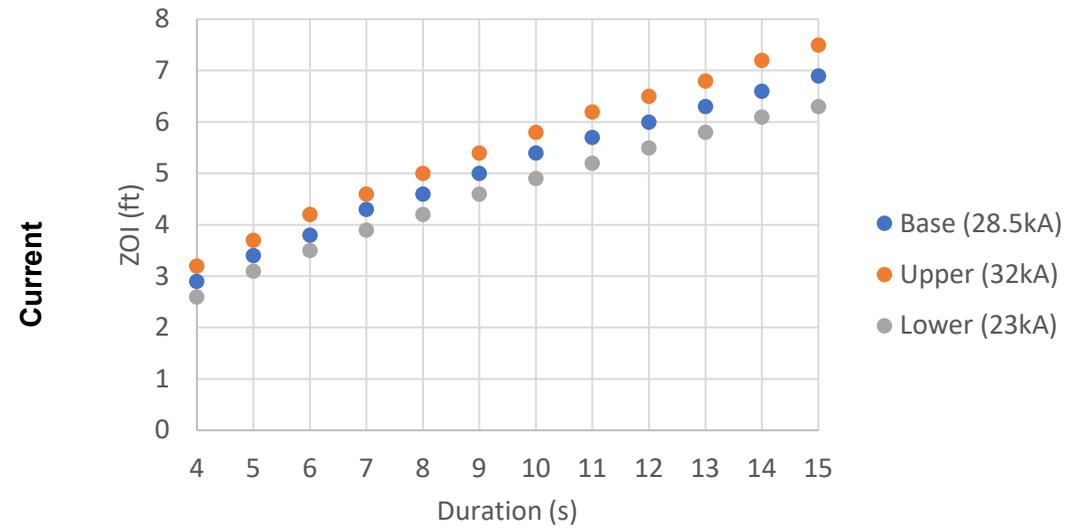
Figure 18. Model Sensitivity Plots (Clockwise from upper left: Current, Conductor Spacing, Volume, and System Voltage.

4 ZONE OF INFLUENCE

This section presents zone of influence (ZOI) estimates for an array of possible HEAF scenarios using the modified model with bias corrections as described in Section 3.4. The ZOIs are listed in tables that are based on the scenario configurations developed by a joint U.S. Nuclear Regulatory Commission Office of Nuclear Regulatory Research (RES) / Electric Power Research Institute (EPRI) HEAF PRA working group. Presenting the results in this way allows for comparison to modeling results develop by the working group using computational fluid dynamic models such as Fire Dynamics Simulator. Tables are presented as follows:

- Switchgear, medium-voltage, steel enclosed (Table 5)
- Switchgear, medium-voltage, aluminum enclosed (Table 6)
- Non-segregated bus ducts, medium-voltage, steel enclosed (Table 7)
- Non-segregated bus ducts, medium-voltage, aluminum enclosed (Table 8)
- Switchgear, low-voltage, steel enclosed (Table 9)
- Switchgear, low-volage, aluminum enclosed (Table 10)

To minimize the breadth of the ZOI tables, the scenarios presented in this section use single point estimates for the arc fault currents, which the NRC-RES/EPRI working group agreed on. While the actual event fault current will be dependent on system configuration and fault conditions, the values used here are expected to be representative and, in some cases, bound plant fault condition observed from operational experience reviews. The durations used in the estimates are based on either a constant current (stiff supply), a decrement current (decaying supply) or a combination of both a constant and decrement current. For the decrement current, the joint working group agreed to a 130MJ decrement curve which resulted in a decrement equivalent arc time of 3.85 seconds. Fault clearing times derived from a plant specific analysis would be used to determine which row of the ZOI tables is applicable for use. In addition, the modified model could be exercised to provide scenario specific ZOIs.

The zone of influence (ZOI) was developed by iterating the model to identify the distance where the incident energy matches the target vulnerability threshold. For cables this is $15MJ/m^2$ for thermoplastic jacketed cable and $30MJ/m^2$ for thermoset jacketed cable. For aluminum enclosed bus ducts with this is $15MJ/m^2$ and $30MJ/m^2$ for bus ducts with steel enclosed. These critical values for incident energy are based on work performed by the Joint NRC/RES – EPRI HEAF Working Group [14].

The modified model does not evaluate the ensuing fire or thermal heat transfer from the thermally hot enclosure. This is beyond the scope of this report but is being addressed by the joint NRC/RES-EPRI HEAF working group and is expected to be published in the future.

Table 6. Medium-voltage Switchgear [30kA, 6.9kV, 0.09in Steel Enclosure]

Fault Duration Stiff (s)	Fault Duration Decrement Equivalent (s)	Equivalent Time (s)	15 MJ/m² (m [ft])	30 MJ/m² (m [ft])
1	0	1	0.3 [1.0]*	0.3 [1.0]*
2	0	2	0.55 [1.8]	0.36 [1.2]
3	0	3	0.76 [2.5]	0.51 [1.7]
4	0	4	0.94 [3.1]	0.62 [2.0]
5	0	5	1.10 [3.6]	0.73 [2.4]
0	3.85	3.85	0.91 [3.0]	0.61 [2.0]
1	3.85	4.85	1.07 [3.5]	0.71 [2.3]
2	3.85	5.85	1.22 [4.0]	0.81 [2.7]
3	3.85	6.85	1.35 [4.4]	0.90 [2.9]
4	3.85	7.85	1.48 [4.8]	0.98 [3.2]
5	3.85	8.85	1.60 [5.2]	1.06 [3.5]

Note: * indicates results are less than the model validation range and the ZOI is limited at 0.3m [1 ft].

Table 7. Medium-voltage Switchgear [30kA, 6.9kV, 0.125 Aluminum Enclosure]

Fault Duration Stiff (s)	Fault Duration Decrement Equivalent (s)	Equivalent Time (s)	15 MJ/m² (m [ft])	30 MJ/m² (m [ft])
1	0	1	0.39 [1.3]	0.3 [1.0]
2	0	2	0.64 [2.1]	0.43 [1.4]
3	0	3	0.84 [2.7]	0.56 [1.8]
4	0	4	1.01 [3.3]	0.67 [2.2]
5	0	5	1.16 [3.8]	0.77 [2.5]
0	3.85	3.85	0.98 [3.2]	0.65 [2.1]
1	3.85	4.85	1.13 [3.7]	0.75 [2.5]
2	3.85	5.85	1.27 [4.2]	0.85 [2.8]
3	3.85	6.85	1.40 [4.6]	0.93 [3.1]
4	3.85	7.85	1.53 [5.0]	1.01 [3.3]
5	3.85	8.85	1.64 [5.4]	1.09 [3.6]

Note: * indicates results are less than the model validation range and the ZOI is limited at 0.3m [1 ft].

Table 8. NSBD Medium-voltage [30kA, 6.9kV, 0.09 Steel Enclosure]

Fault Duration Stiff (s)	Fault Duration Decrement Equivalent (s)	Equivalent Time (s)	15 MJ/m² (m [ft])	30 MJ/m² (m [ft])
1	0	1	0.3 [1.0]*	0.3 [1.0]*
2	0	2	0.39 [1.3]	0.3 [1.0]*
3	0	3	0.54 [1.8]	0.35 [1.1]
4	0	4	0.67 [2.2]	0.43 [1.4]
5	0	5	0.79 [2.6]	0.51 [1.7]
0	3.85	3.85	0.65 [2.1]	0.42 [1.4]
1	3.85	4.85	0.77 [2.5]	0.50 [1.6]
2	3.85	5.85	0.88 [2.9]	0.57 [1.9]
3	3.85	6.85	0.99 [3.2]	0.63 [2.1]
4	3.85	7.85	1.08 [3.6]	0.70 [2.3]
5	3.85	8.85	1.18 [3.9]	0.76 [2.5]

Note: * indicates results are less than the model validation range and the ZOI is limited at 0.3m [1 ft].

Table 9. NSBD Medium-voltage [30kA, 6.9kV, 0.125 Aluminum Enclosure]

Fault Duration Stiff (s)	Fault Duration Decrement Equivalent (s)	Equivalent Time (s)	15 MJ/m² (m [ft])	30 MJ/m² (m [ft])
1	0	1	0.3 [1.0]*	0.3 [1.0]*
2	0	2	0.44 [1.4]	0.3 [1.0]*
3	0	3	0.58 [1.9]	0.38 [1.2]
4	0	4	0.71 [2.3]	0.46 [1.5]
5	0	5	0.83 [2.7]	0.53 [1.7]
0	3.85	3.85	0.69 [2.3]	0.45 [1.5]
1	3.85	4.85	0.81 [2.7]	0.52 [1.7]
2	3.85	5.85	0.92 [3.0]	0.59 [1.9]
3	3.85	6.85	1.02 [3.3]	0.65 [2.1]
4	3.85	7.85	1.11 [3.7]	0.72 [2.3]
5	3.85	8.85	1.20 [4.0]	0.77 [2.5]

Note: * indicates results less than the model validation range and the ZOI is limited at 0.3m [1 ft].

Table 10. Low-voltage Switchgear [32kA, 0.6kV, 0.09 Steel Enclosure]

Current (kA)	Fault Duration Decrement Equivalent (s)	15 MJ/m² (m [ft])	30 MJ/m² (m [ft])
32.0	1	0.3 [1.0]*	0.3 [1.0]*
32.0	2	0.36 [1.2]	0.3 [1.0]*
32.0	3	0.48 [1.6]	0.34 [1.1]
32.0	4	0.58 [1.9]	0.41 [1.4]
32.0	5	0.66 [2.2]	0.47 [1.5]
32.0	6	0.74 [2.4]	0.52 [1.7]
3.4	40	0.57 [1.9]	0.41 [1.3]

Note: * indicates results less than the model validation range and the ZOI is limited at 0.3m [1 ft].

Table 11. Low-voltage Switchgear [32kA, 0.6kV, 0.125 Aluminum Enclosure]

Current (kA)	Fault Duration Decrement Equivalent (s)	15 MJ/m² (m [ft])	30 MJ/m² (m [ft])
32.0	1	0.3 [1.0]*	0.3 [1.0]*
32.0	2	0.44 [1.4]	0.31 [1.0]
32.0	3	0.54 [1.8]	0.39 [1.3]
32.0	4	0.63 [2.1]	0.45 [1.5]
32.0	5	0.71 [2.3]	0.50 [1.6]
32.0	6	0.77 [2.5]	0.55 [1.8]
3.4	40	0.62 [2.0]	0.44 [1.4]

Note: * indicates results less than the model validation range and the ZOI is limited at 0.3m [1 ft].

5   SUMMARY

The report documents the evaluation, modification and application of an approach to predict the arcing hazard from high energy arcing faults (HEAFs) involving aluminum. Gaps between the underlying assumptions and intended application of an initial model were identified and addressed to improve the prediction capabilities. These modifications were based on existing literature and available test data. The modified model was then exercised in conjunction with target fragility thresholds to develop zone of influence estimates to support refinements in fire PRA methods. The results from this work are expected to be used in conjunction with other efforts under development by the U.S. Nuclear Regulatory Commission (NRC) Office of Nuclear Regulatory Research (RES) and Electric Power Research Institute (EPRI) joint working group on HEAF. The end user is reminded that the information presented in this report is not regulatory guidance, nor does it represent regulatory requirements.

6   REFERENCES[1]

1.   Information Notice 2017-04, "High Energy Arcing Faults in Electrical Equipment Containing Aluminum Components," ADAMS Accession No. ML17058A343 U.S. Nuclear Regulatory Commission, Washington, DC 20555-0001, August 2017.

2.   NUREG/CR-6850, EPRI 1011989, "EPRI/NRC-RES Fire PRA Methodology for Nuclear Power Facilities: Volume 2: Detailed Methodology." Electric Power Research Institute (EPRI), Palo Alto, CA, and U.S. Nuclear Regulatory Commission, Washington DC 20555-0001, 2005 .

3.   NEA OECD Fire Project – Topical Report No. 1, *Analysis of High Energy Arcing Fault (HEAF) Fire Events*¸ Nuclear Energy Agency, Committee on The Safety of Nuclear Installations, Organization for Economic Cooperation and Development, June 2013.

4.   NEA HEAF Project – TOPICAL REPORT No. 1, *Experimental Results from the International High Energy Arcing Fault (HEAF) Research Program – Phase 1 Testing 2014 to 2016,* Nuclear Energy Agency, Committee on The Safety of Nuclear Installations, Organization for Economic Cooperation and Development, May 2017.

5.   Memorandum, "Submittal of Possible Generic Issue Concerning the Damage Caused by High Energy Arc Faults in Electrical Equipment containing Aluminum Components," U.S. Nuclear Regulatory Commission, Washington, DC 20555-0001, (ADAMS Accession No. ML16126A096), May 2016.

6.   Memorandum, Results of Generic Issue Review Panel Screening Evaluation for Proposed Generic Issue Pre-GI-018, High Energy Arc Faults involving Aluminum (ADAMS Accession No. ML16349A027). Washington, DC 20555-0001, July 2017

7.   Assessment Plan for Pre-GI-018, Proposed Generic Issue on High Energy Arc Faults Involving Aluminum (ADAMS Accession No. ML18172A185). Washington, DC, August 2018.

8.   Update to the Assessment Plan for Pre-GI-018, Proposed Generic Issue on High Energy Arc Faults Involving Aluminum (ADAMS Accession No. ML19127A202). Washington, DC, July 2019.

9.   Memorandum from R. Furstenau to A.D. Veil regarding Closure of Proposed Generic Issue PRE-GE-018 High Energy Arc Faults Involving Aluminum, (ADAMS Accession No. ML21237A360), U.S. Nuclear Regulatory Commission, Washington DC, April 2021.

10.   Integrated Risk-Informed Decision-making Process for Emergent Issues, (ADAMS Accession No. ML19253D401), U.S. Nuclear Regulatory Commission, Washington DC, March 2020.

11.   IEEE 1584-2018, IEEE Guide for Performing Arc-Flash Hazard Calculations. New York: The Institute of Electrical and Electronic Engineers, Inc., New York, NY, 2018.

12.   Lee, Ralph H. "The Other Electrical Hazard: Electric Arc Blast Burns." IEEE Transactions on Industry Applications 246-251, 1982.

13.   IEEE 1584-2002, IEEE Guide for Performing Arc-Flash Hazard Calculations. New York: Institute of Electrical and Electronic Engineers, Inc, New York, NY, 2002.

14.   Target Fragilities for Equipment Vulnerable to High Energy Arcing Faults," (ADAMS accession No. ML22131A339), U.S. Nuclear Regulatory Commission, Washington, DC 20555-0001 and Electric Power Research Institute, Palo Alto, CA, May 2022.

15.   NUREG-1824, Verification and Validation of Selected Fire Models for Nuclear Power

---

[1] Publicly available NRC published documents are available electronically through the NRC Library on the NRC's public Web site at http://www.nrc.gov/reading-rm/doc-collections/. The documents can also be viewed online or printed for a fee in the NRC's Public Document Room (PDR) at 11555 Rockville Pike, Rockville, MD; the mailing address is USNRC PDR, Washington, DC 20555; telephone (301) 415-4737 or (800) 397-4209; fax (301) 415-3548; and e-mail pdr.resource@nrc.gov.

Plant Applications (Supplement 1). NUREG, Washington DC / Palo Alto, CA: U.S. Nuclear Regulatory Commission / Electric Power Research Institute, 2016.

16.   RIL 2021-10, "Report on High Energy Arcing Fault Experiments, Experimental Results from Medium Voltage Electrical Enclosures," U.S. Nuclear Regulatory Commission, Washington, DC 20555-0001, NIST TN 2188, National Institute of Standards and Technology, Gaithersburg, MD, SAND2021-12049R, Sandia National Laboratories, Albuquerque, NM, 2021.

17.   RIL 2021-18, "Report on High Energy Arcing Fault Experiments, Experimental Results from Open Box Enclosures," U.S. Nuclear Regulatory Commission, Washington, DC 20555-0001, NIST TN 2198, National Institute of Standards and Technology, Gaithersburg, MD, SAND2021-16075 R, Sandia National Laboratories, Albuquerque, NM, 2021.

18.   RIL 2021-17, "Report on High Energy Arcing Fault Experiments, Experimental Results from Low Voltage Electrical Enclosures," U.S. Nuclear Regulatory Commission, Washington, DC 20555-0001, NIST TN 2197, National Institute of Standards and Technology, Gaithersburg, MD, 2021.

19.   Babusci, G., et. al., "Assessment of the Behavior of gas-insulted Electrical Components in the Presence of Arc," 1998.

20.   Bernard, G., "Electrical faults mastery in high voltage SF_6 insulated substations," EDF, 1982.

21.   Trinh, N.G., "Evaluation of the Risk of Burn through due to Internal Arc of Gas-Insulated Equipment," CEA Trans, March 1989.

22.   Boeck, W.A., and Kruger, K., "Arc motion and burn through in GIS," IEEE Transactions on Power Delivery, Vol. 7, p 254-261, 1992.

23.   Chu, F., et. al., Estimation of Burn-Through Probability in SF_6 insulated substations," Power Apparatus and Systems, IEEE Transactions, PAS-101, 1391-1399, 1982.

24.   EPRI 3002015992, "Nuclear Station Electrical Distribution Systems and High-Energy Arcing Faults Events," Electric Power Research Institute, Palo Alto, CA, July 2019.

25.   CIGRE 602, Tools for the simulation of the effects of the internal arc in transmission and distribution switchgear. ISBN: 978-2-85873-303-3, CIGRE, 2014.

APPENDIX A
ARC VOLTAGE

Arc voltage is an important parameter for determining arc energy and for the time to breach and time to open model modification. The arc voltage is the voltage drop of an arc between the arc roots. Arc voltage varies because of arc looping, change in electrode configuration, compartment size, and pressure. Arc voltage is different from system voltage as shown in Figure 19. The arc is highly resistive and as such has a dependency on resistivity and arc current. While arc voltage is not an input to the model, it is used to calculate the energy of specific HEAF PRA scenarios and for the breach adjustment approach. Thus, the arc voltage needs to be known or estimated. The following provides a review of the evidence available to estimate the arc voltage for different voltage classes of equipment.
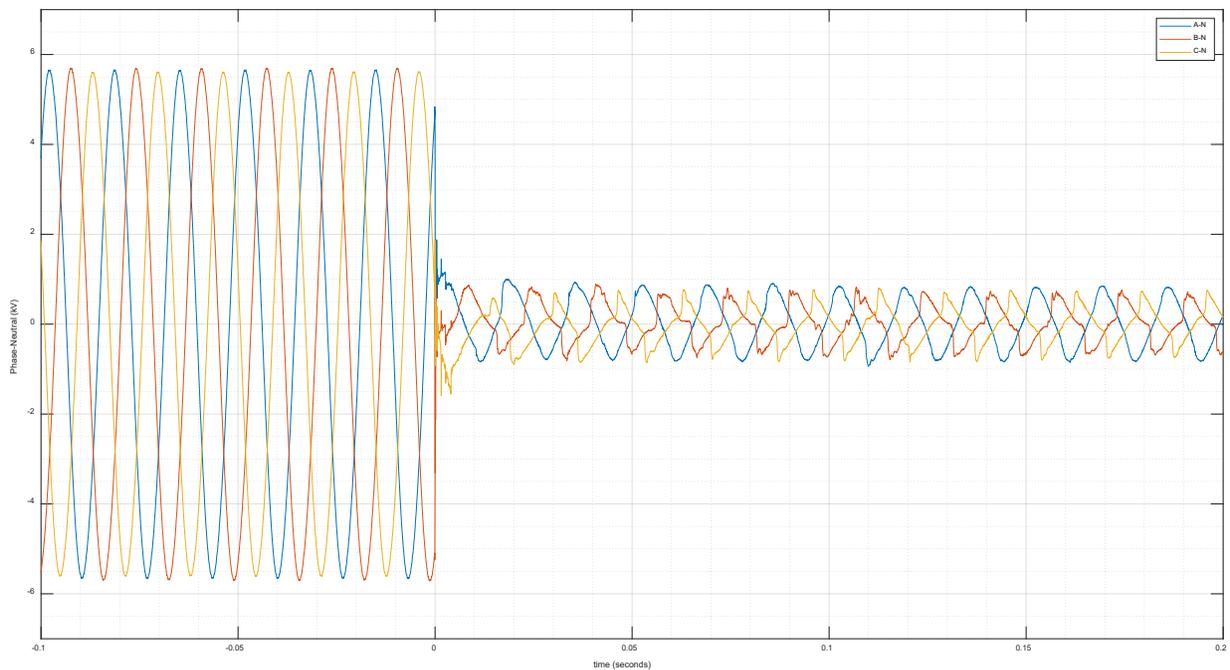

Figure 19. Voltage Profile prior to (System Voltage) and during (Arcing Voltage) initial arcing duration (Voltage shown as Phase Voltage)

A.1 Test data

The test data is limited due to the varying locations where the voltage measurements were made. Arc voltages were acquired for the low-voltage switchgear [18] and low-voltage box tested in 2019 [17]. The switchgear bus spacing on center is 5-inches and the box bus spacing on center is 3.5-inches. These results are presented in Table 11 and Figure 20. The low-voltage switchgear shows a slightly higher arc voltage than the box enclosure but comparison between the two test configurations show a 95% confidence interval for the mean to only vary 10-20 volts between the two. Thus, these similarities suggest combining the two data sets, which results in a mean of $350V_{L-L}$ and an 95% confidence interval for the mean of 320 V_{L-L} to $375V_{L-L}$. Based on this a mean of $350V_{L-L}$ for low-voltage equipment is suggested. If conservatism in the estimate is needed the upper value of $375V_{L-L}$ could be used for low-voltage equipment.

Table 12. Arc Voltage Measurements for Low-voltage Tests

Test ID LV SwGr	Current (kA)	System Voltage (V_{L-L})	Arc Voltage (V_{L-L})	Test ID LV Box	Current (kA)	System Voltage (V_{L-L})	Arc Voltage (V_{L-L})
2-13A	9.800	480	389	OB01a	1.052	1,000	347
2-13B	9.973	600	420	OB01b	1.030	1,000	308
2-13C	11.650	600	298	OB02	14.016	1,000	271
2-13D	9.266	600	426	OB03	13.804	1,000	314
2-13E (Cu)	10.388	600	305	OB04	27.786	1,000	276
2-13F	9.733	480	302	OB05	1.018	1,000	359
2-13G	10.707	600	330	OB06	11.959	1,000	424
2-18A	19.146	480	290	OB07	12.952	1,000	431
2-18B	19.349	600	415	OB08*	24.870	1,000	537*
				OB09	4.794	1,000	297
				OB10	4.869	1,000	381
Average			353	**Average**			341*
Maximum			426	**Maximum**			431*

* Rod ejection resulted in abnormal arc voltage during Test OB08 and removed
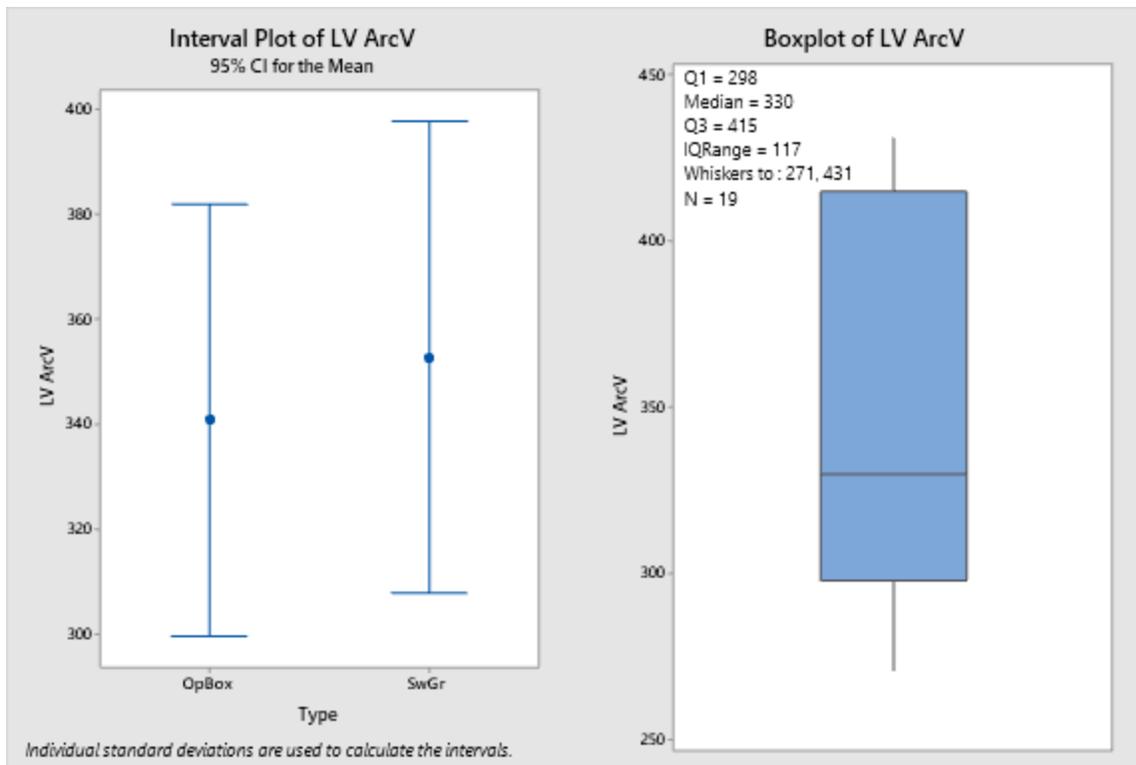
Figure 20. Interval Plot (left) and Box Plot (right) of LV Arc Voltage Data

The medium-voltage tests did not include an arc voltage measurement for the 2018 switchgear tests. The only voltage measurement was made at the generator and voltage losses between the generator and the test device cannot be estimated. The medium-voltage open box tests did measure voltage at the test device [17]. The available medium-voltage data is presented below.

Table 13. Voltage Measurements for Medium-voltage Tests

Test ID MV SwGr	Current (kA)	System Voltage (kV$_{L-L}$)	Gen Voltage (V$_{L-L}$)	Test ID MV Box	Current (kA)	System Voltage (kV$_{L-L}$)	Gen Voltage (V$_{L-L}$)	Arc Voltage (V$_{L-L}$)
2-19 (AL)	25.8	6.9	767	OBMV01 (AL)	14.3	6.9	623	543
2-21 (AL)	26.6	6.9	769	OBMV02 (AL)	29.1	6.9	830	468
2-22 (AL)	32.0	7.0	869	OBMV03 (AL)	14.4	6.9	606	475
2-24 (AL)	29.8	7.0	876	OBMV04 (CU)	14.3	6.9	597	458
				OBMV05 (CU)	28.6	6.9	775	406
				OBMV06 (AL)	14.6	6.9	671	493
Average			820	Average			683	475
Maximum			876	Maximum			830	543

A.2   Arc voltage model

There are several models available for estimating arc voltage. The predominant models are presented below with reference to the NRC test data of known arc voltage measurements.

CIGRE 602, "Tools for the Simulation of the Effects of the Internal Arc in Transmission and Distribution Switchgear [25]" presents a model for estimating arc voltage. For MV metal enclosed switchgear in air with copper electrodes, the arc voltage can be estimated as,

$$\frac{U_{arc}}{d} = 30\frac{V}{cm} + \frac{1}{2}I_{rms}\frac{V}{cm\ kA} \le 40\frac{V}{cm}$$

where, U_{arc}, phase-to-phase (LL) arc voltage (volts)
                d, distance between electrode centers (cm)
                I_{rms}, the effective short circuit current (kA)

Using the arc voltage measurements available, the model is compared for low-voltage and medium-voltage as shown in Figure 21.
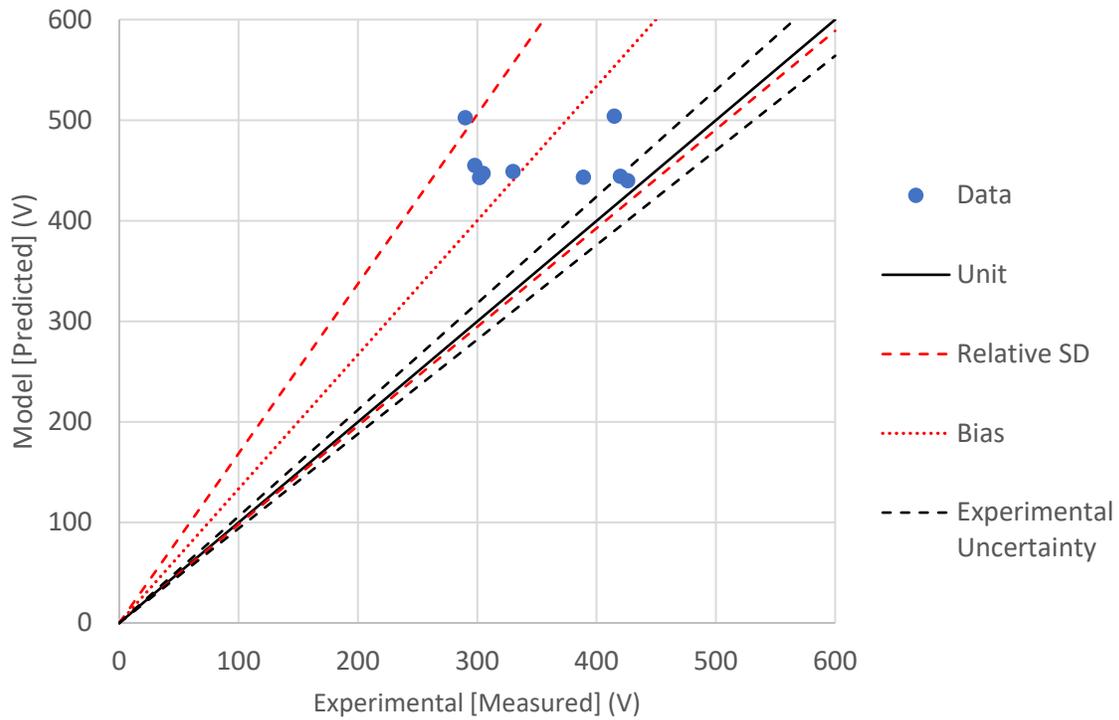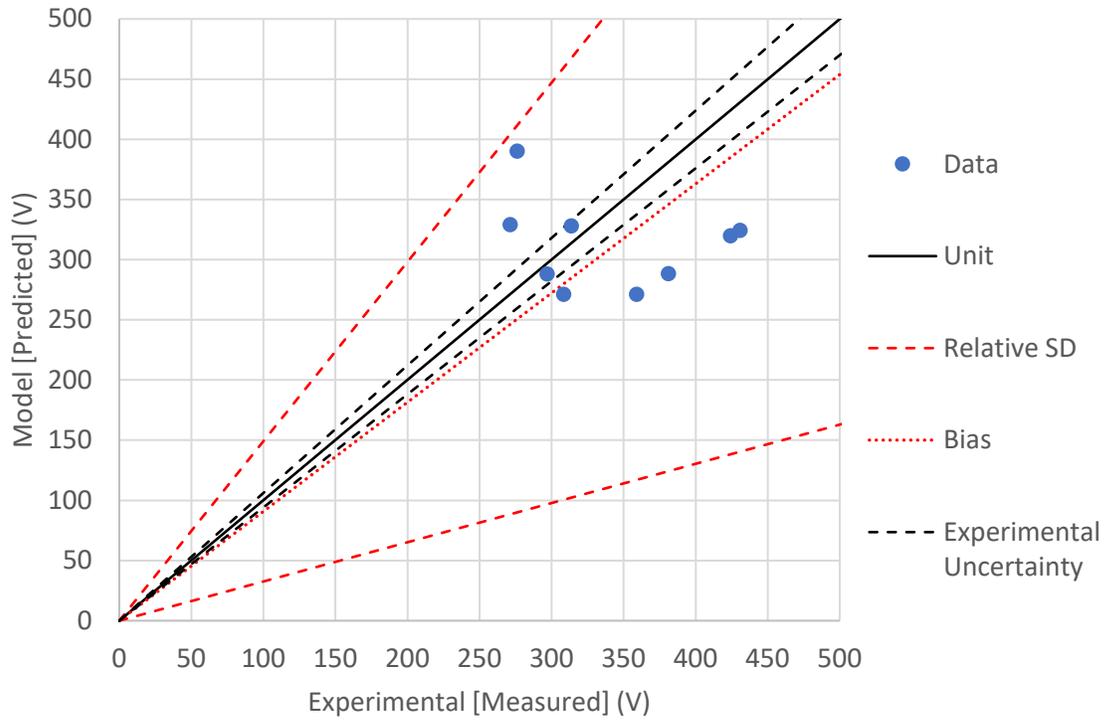
Figure 21. Model evaluation for Low-voltage box tests (Top) and Low-voltage Switchgear voltage (Bottom) to the CIGRE 602 arc voltage model. All voltage shown are Line-to-Line. [Top - Low-voltage box Bias = 0.91, SD_M=0.29] [Bottom - Low-voltage switchgear Bias = 1.33, SD_M=0.18]
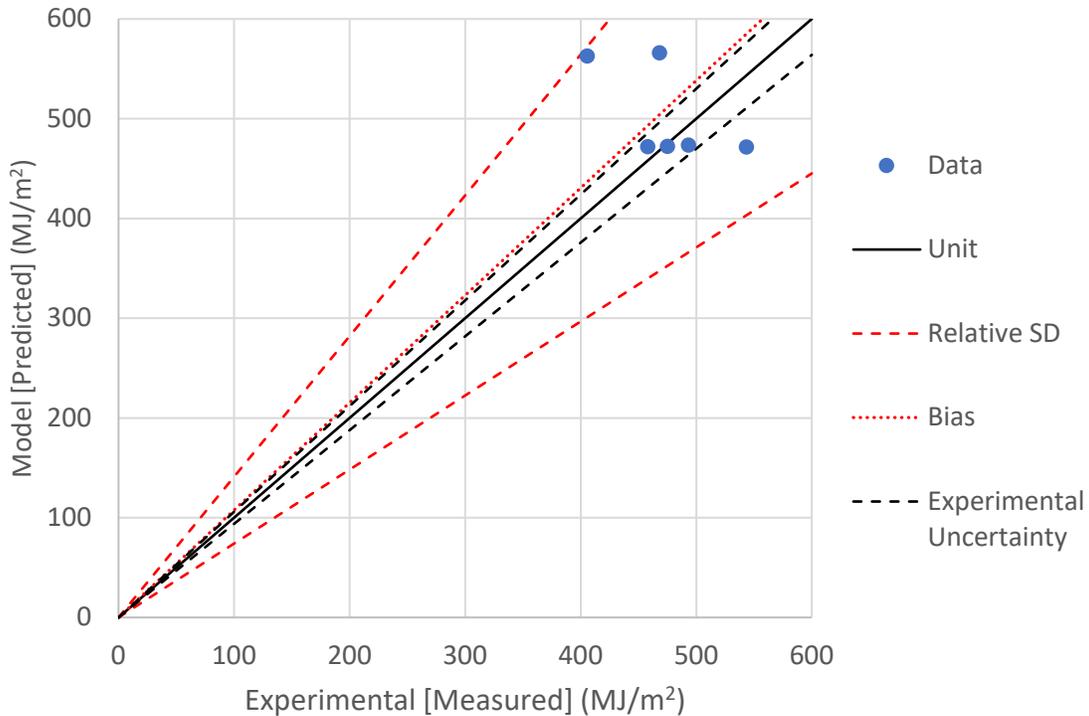
Figure 22. Model Evaluation for Medium-voltage box tests to the CIGRE 602 arc voltage model [Medium-voltage Bias = 1.08, SD_M=0.17]

The box tests bus bar spacing for medium-voltage equipment was smaller than the 2018 MV switchgear tests. Since measurements of arc voltage were not made during the 2018 test series, the arc voltage is estimated for those tests as shown below using the CIGRE model and correction factor (1.08). Using this information to correct the CIGRE 602 model prediction, the arc voltage was estimated for each of the 2018 tests with the results presented in Table 13. From this a representative value to use for medium-voltage is $650V_{LL}$.

Table 14. CIGRE 602 estimates of arc voltage for 2018 tests

Test ID	I_{rms} (kA)	U_{gen} (V_{LL}) measured	U_{arc} (V_{LL})	U_{arc} (VLL) corrected
2-19	25.8	767	681	631
2-21	26.6	769	687	636
2-22	32.0	869	730	676
2-24	29.8	876	713	660
			Average	650 V_{L-L} [375 V_{L-N}]
			Maximum	676 V_{L-L} [390 V_{L-N}]
			3rd Quartile	665 V_{L-L} [384 V_{L-N}]

APPENDIX B
ZOI TABLE MODELING INPUT

This appendix documents the input parameters that were used to calculate the zone of influence (ZOI) presented in Section 4.

B.1 Non-segregated phase bus duct

Based on equipment procured for testing as specified by NRC-RES/EPRI Working Group as being garden variety bus duct, shown in Figure 23. Enclosure thickness is 11Ga (3.2mm [1/8 in]) steel or (2.3mm [0.091 in]) aluminum. Model parameters are shown in Figure 24. Note that the time and critical incident energy values were varied to the specific scenario. Critical incident energy values were either 15 MJ/m^2 or 30 MJ/m^2 dependents on the target. The enclosure type steel or aluminum was also evaluated. VCB configuration was used as this would postulate damage to targets above or below the bus duct.
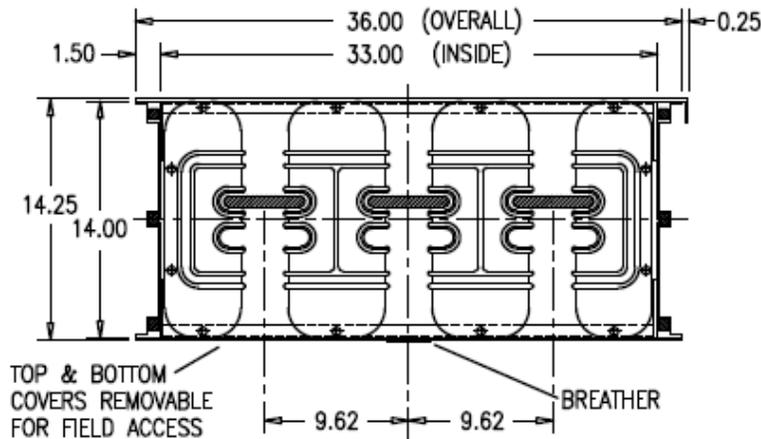

**Figure 23. Bus Duct Specification (Aluminum bus and duct)**

INPUT PARAMETERS

Conductor Gap Spacing	G	3.63	in
Arc Fault Current	I_{arc}	30	kA
Configuration		VCB	
Open Circuit Voltage	V_{oc}	6.9	kV
Duration	T	Varied	seconds
Enclosure Width	W	33	in
Enclosure Height	H	36	in
Enclosure Depth	D	14.25	in
Critial Incident Energy	IE	15 or 30	MJ/m^2
Enclosure Type		Typical	
Bolted Fault Current	I_{bf}	34.18	kA

Enclosure Thickness	0.09	in
Enclosure Material	Steel	
Enclosure Zone	LV Switchgear	

Figure 24. Input Parameters for non-segregated bus duct.

B.2   Zone 1 and 2 MV Switchgear

Based on equipment tested during the 2018 MV Switchgear tests, shown in Figure 25. Enclosure exterior panel thickness is 13 Ga (2.3mm [0.09 in]) steel. Model parameters are shown in Figure 26. Note that the time and critical incident energy values were varied to the specific scenario. Critical incident energy values were either 15 MJ/m^2 or 30 MJ/m^2 dependents on the target. The enclosure type steel was the only one evaluated. Configuration selected was dependent on the equipment type location. For the supply vertical section, the VCB configuration was used. For the Load and Main Bus Vert Section, the HCB was selected since this representative of the load configuration and bounding for the main bus.
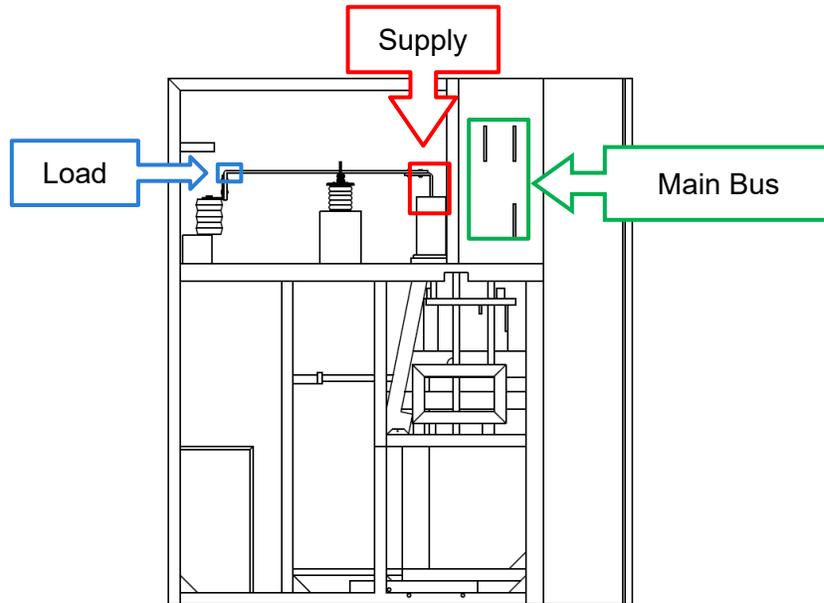
Figure 25. Medium-voltage Switchgear

INPUT PARAMETERS

| Conductor Gap Spacing	G	6.02	in
Arc Fault Current	I_{arc}	30	kA
Configuration		HCB	
Open Circuit Voltage	V_{oc}	6.9	kV
Duration	T	Varied	seconds
Enclosure Width	W	36	in
Enclosure Height	H	36	in
Enclosure Depth	D	36	in
Critial Incident Energy	IE	15 or 30	MJ/m^2
Enclosure Type		Typical	
Bolted Fault Current	I_{bf}	34.51	kA
Enclosure Thickness		0.09	in
Enclosure Material		Steel	
Enclosure Zone		MV Switchgear	

Figure 26. Input Parameters for Zone 1 and 2 MV Switchgear

B.3   Zone 3 LV Switchgear

Based on equipment tested during the 2019 LV Switchgear tests, shown in Figure 25. Enclosure exterior panel thickness is 13 Ga (2.3mm [0.09 in]) steel. Model parameters are shown in Figure 28. Note that the time and critical incident energy values were varied to the specific scenario. Critical incident energy values were either 15 MJ/m^2 or 30 MJ/m^2 dependents on the target. The enclosure type steel was the only one evaluated. Configuration selected was dependent on the equipment type location. For the supply vertical section, the VCB configuration was used. For the Load and Main Bus Vert Section, the HCB was selected since this representative of the load configuration and bounding for the main bus.
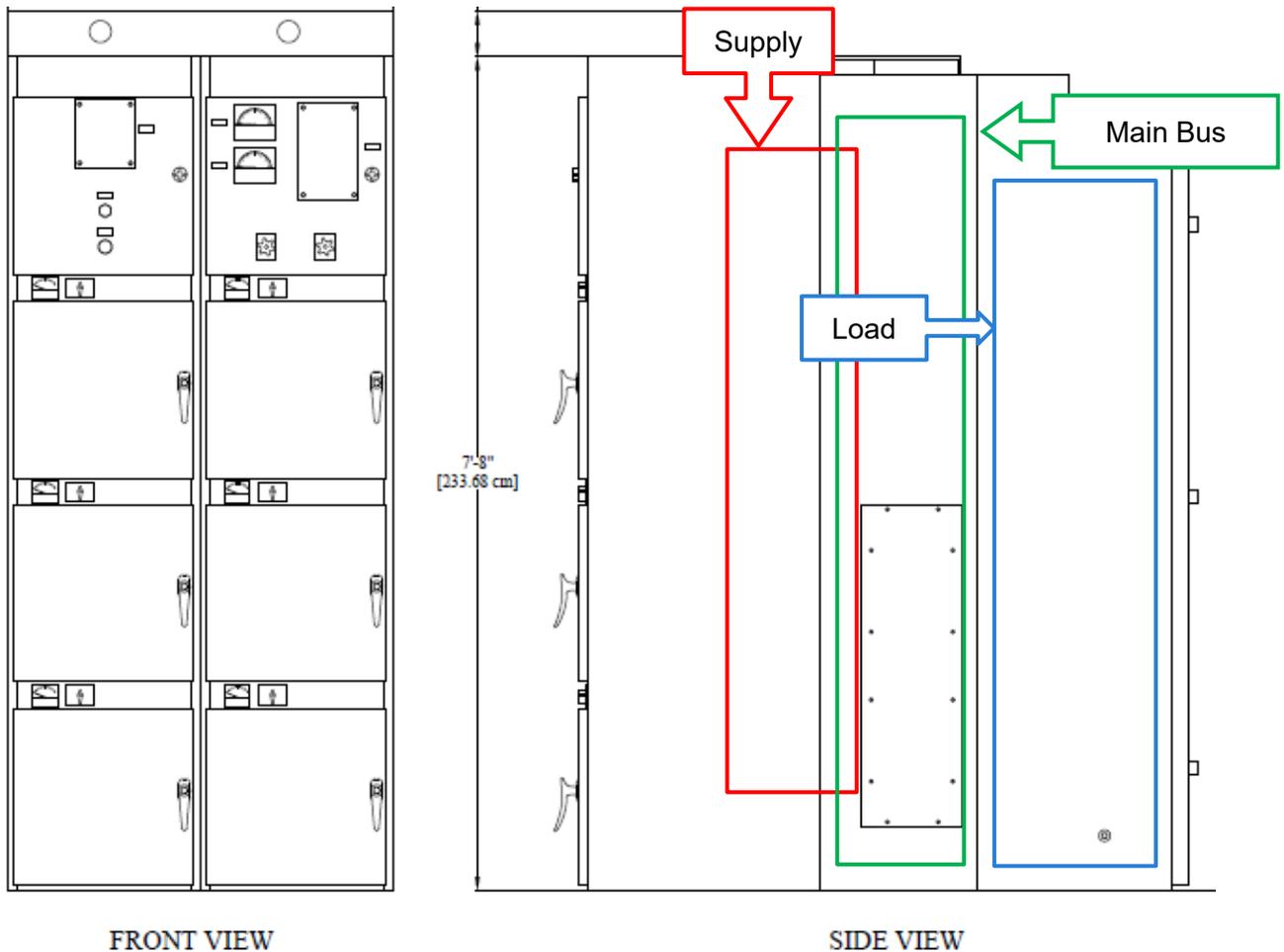

Figure 27. Low-voltage switchgear

INPUT PARAMETERS

Conductor Gap Spacing	G	1.26	in
Arc Fault Current	I_{arc}	32	kA
Configuration		HCB	
Open Circuit Voltage	V_{oc}	0.6	kV
Duration	T	Varied	seconds
Enclosure Width	W	24	in
Enclosure Height	H	24	in
Enclosure Depth	D	14	in
Critial Incident Energy	IE	15 or 30	MJ/m^2
Enclosure Type		Typical	
Bolted Fault Current	I_{bf}	45.06	kA

|		
Enclosure Thickness	0.09	in
Enclosure Material	Steel	
Enclosure Zone	LV Switchgear	

Figure 28. Input Parameters for Zone 3 LV Switchgear.